UNIVERSITY OF CALIFORNIA, SAN DIEGO

Tracking marine mammals and ships with small and large-aperture hydrophone arrays

A dissertation submitted in partial satisfaction of the
requirements for the degree of Doctor of Philosophy

in

Electrical Engineering (Applied Ocean Sciences)

by

Martin Gassmann

Committee in charge:

Professor John Hildebrand, Chair
Professor William Hodgkiss, Co-Chair
Professor Jay Barlow
Professor Michael Buckingham
Professor Gert Lanckriet
Professor Marie Roch

2015

The Dissertation of Martin Gassmann is approved and is acceptable in quality and form for publication on microfilm and electronically:

_____

_____

_____

_____

_____
Co-Chair

_____
Chair

University of California, San Diego

2015

DEDICATION

To my Mom.

TABLE OF CONTENTS

LIST OF FIGURES

LIST OF TABLES

ACKNOWLEDGEMENTS

I would like to express my gratitude to all who helped and supported me to grow in many ways during the PhD program; not only as a scientist and engineer, but also as a person.

A natural place to start is with my adviser Dr. John Hildebrand to whom I'm deeply indebted. Not only is John the man, who got me excited about the combination of engineering and oceanography, but he also opened up to me the adventurous possibility to pursue this challenging PhD at this top-ranked university in San Diego, California. I'm deeply grateful to John for his great confidence in me and tremendous support during both, the good and the tough times in my life, while in the PhD program. His holistic, 'big picture' approach that also includes non-academic matters and his excellent physical intuition helped me tremendously to learn, grow and succeed during the PhD program.

Furthermore, I would like to extend my gratitude to my committee members: my co-adviser Dr. Bill Hodgkiss for his eloquent and excellent teaching of signal processing and his critical advice for my research, Dr. Mike Buckingham for extremely helpful mathematical discussions about underwater acoustics and signal processing infused with truly pleasant and uplifting conversations not only about flying, Dr. Marie Roch for all her support, Dr. Jay Barlow for reminding me to keep the 'biology' in mind and Dr. Gert Lanckriet for his willingness to serve on this committee.

In addition, I would like to thank the Scripps Whale Acoustic Lab, especially Dr. Sean Wiggins. Although Sean did not formally served on my committee, I'm also deeply indebted to him as he provided critical advice and support throughout my PhD and also helped me tremendously to learn, grow and succeed in the good and in the tough times during the program.

I also would like to thank the University of California ship fund for young investigators, especially Dr. Bruce Applegate, for providing the adventurous experience

of leading a research cruise on R/V Robert Gordon Sproul as the chief scientist to recover the acoustic dataset for chapter 3 and 4 of this dissertation. In addition, I thank the captain and crew of R/V Sproul for supporting the field work during several cruises.

My gratitude is also deeply indebted to my Dad, my brother David and especially my Mom, to whom this dissertation is dedicated and whose motherly love and faith continues to inspire me to set and achieve higher and noble goals in life such as earning this PhD degree.

Naturally, I'm also deeply grateful to my wonderful wife Ewa for her amazing love, her great faith in me and all the sacrifices she made, in good times and in bad times, to help me to earn this PhD degree.

Finally, I would like to express my gratitude to all the great people from all over the world that I enjoyed meeting during my PhD and the many that I became friends with, in particular with John Paul. My friendship with this amazing and wise, but yet very loving, joyful and humble man has helped me enormously to grow in so many ways.

Chapter 2, in full, is a reprint of the material as it appears in Gassmann, M., Henderson, E. E., Wiggins, S. M., Roch, M. A., and Hildebrand, J. A. (2013). Offshore killer whale tracking using multiple hydrophone arrays. *The Journal of the Acoustical Society of America*, 134(5):35133521. The dissertation author was the primary investigator and author of this paper.

Chapter 3, in full, has been accepted for publication of the material as it will appear in Gassmann, M., Wiggins, S. M., and Hildebrand, J. A. Three-dimensional tracking of Cuvier's beaked whales' echolocation sounds using nested hydrophone arrays. *The Journal of the Acoustical Society of America*, in press. The dissertation author was the primary investigator and author of this paper.

Chapter 4 is currently being prepared for submission for publication of the material. Gassmann, M., Wiggins, S. M., and Hildebrand, J. A. Tracking and measuring underwater radiated sound from ships with a small-aperture seafloor array. The dissertation author was the primary investigator and author of this paper.

VITA

2015 Doctor of Philosophy in Electrical Engineering (Applied Ocean Sciences), University of California, San Diego, USA

2010 Diplom-Ingenieur Elektrotechnik, Universität Rostock, Germany

AWARDS

2013 Best poster in electrical and computer engineering, Jacobs School of Engineering Research Expo, University of California, San Diego

2011 Best paper by a young investigator in signal processing in acoustics, Acoustical Society of America, San Diego meeting

2011 University of California Young Investigator ship fund for ship time on R/V Robert Gordon Sproul

PUBLICATIONS

Gassmann, M., Wiggins, S. M., and Hildebrand, J. A. Three-dimensional tracking of Cuvier's beaked whales' echolocation sounds using nested hydrophone arrays. *The Journal of the Acoustical Society of America*, in press.

Gassmann, M., Henderson, E. E., Wiggins, S. M., Roch, M. A., and Hildebrand, J. A. (2013). Offshore killer whale tracking using multiple hydrophone arrays. *The Journal of the Acoustical Society of America*, 134(5):35133521.

Henderson, E. E., Smith, M. H., Gassmann, M., Wiggins, S. M., Douglas, A. B., and Hildebrand, J. A. (2014). Delphinid behavioral responses to incidental mid-frequency active sonar. *The Journal of the Acoustical Society of America*, 136(4):20032014.

Simonis, A. E., Baumann-Pickering, S., Oleson, E., Melcon, M. L., Gassmann, M., Wiggins, S. M., and Hildebrand, J. A. (2012). High-frequency modulated signals of killer whales (orcinus orca) in the north pacific. *The Journal of the Acoustical Society of America*, 131(4):EL295EL301.

ABSTRACT OF THE DISSERTATION

Tracking marine mammals and ships with small and large-aperture hydrophone arrays

by

Martin Gassmann

Doctor of Philosophy in Electrical Engineering (Applied Ocean Sciences)

University of California, San Diego, 2015

Professor John Hildebrand, Chair
Professor William Hodgkiss, Co-Chair

Techniques for passive acoustic tracking in all three spatial dimensions of marine mammals and ships were developed for long-term acoustic datasets recorded continuously over months using custom-designed arrays of underwater microphones (hydrophones) with spacing ranging from meters to kilometers.

From the three-dimensional tracks, the acoustical properties of toothed whales and ships, such as sound intensity and directionality, were estimated as they are needed for the passive acoustic abundance estimation of toothed whales and for a quantitative description of the contribution of ships to the underwater soundscape. In addition, the

tracks of the toothed whales reveal their underwater movements and demonstrate the potential of the developed tracking techniques to investigate their natural behavior and responses to sound generated by human activity, such as from ships or military SONAR.

To track the periodically emitted echolocation sounds of toothed whales in an acoustically refractive environment in the upper ocean, a propagation-model based technique was developed for a hydrophone array consisting of one vertical and two L-shaped subarrays deployed from the floating instrument platform R/P FLIP. The technique is illustrated by tracking a group of five shallow-diving killer whales showing coordinated behavior.

The challenge of tracking the highly directional echolocation sounds of deep-diving (< 1 *km*) toothed whales, in particular Cuvier's beaked whales, was addressed by embedding volumetric small-aperture (≈ 1 *m* element spacing) arrays into a large-aperture (≈ 1 *km* element spacing) seafloor array to reduce the minimum number of required receivers from five to two. The capabilities of this technique are illustrated by tracking several groups of up to three individuals over time periods from 10 *min* to 33 *min* within an area of 20 km^2 in the Southern California Bight.

To track and measure the underwater radiated sound of ships, a frequency domain beamformer was implemented for a volumetric hydrophone array (< 2 *m* element spacing) that was coupled to an autonomous acoustic seafloor recorder. This allows for the tracking and measurement of underwater radiated sound from ships of opportunity with a single-instrument deployment and without depending on track information from the automatic information system (AIS).

Chapter 1

Introduction

When compared to light, sound propagates well in the ocean since its attenuation in sea water due to absorption is small (Medwin and Clay, 1998). This allows the acoustic pressure waves to travel large distances of up to several thousands of kilometers depending upon their wavelengths and the oceanic environment.

Therefore, a variety of natural processes in the oceanic environment are able to contribute to the underwater acoustic soundscape at a given location. Besides physical processes such as surface agitation, marine organisms are naturally a significant component of the underwater acoustic soundscape and utilize sound for a wide range of tasks (Wenz, 1962). For example, marine mammals produce frequently sounds for communication and navigation purposes. While large baleen whales, such as blue whales, emit long sound waves (equivalent to low sound frequencies) that can travel across ocean basins allowing for long-range communication with their conspecifics (Edds-Walton, 1997), toothed whales, such as killer whales, produce short sounds with short wavelengths (equivalent to high sound frequencies) for navigation purposes, which are received at distances up to tens of kilometers only (Au, 1993).

In addition to natural processes, anthropogenic sound generated by human-related activities in the oceanic environment contributes also to the underwater acoustic soundscape (Hildebrand, 2009). This includes underwater sound that is intentionally generated,

e.g. for oil and gas exploration or for underwater warfare, as well as sound that is generated as a by-product of human activity, e.g. from commercial shipping. As the ocean is being increasingly utilized, a quantitative description of the natural and anthropogenic contributions to the underwater acoustic soundscape is needed to understand the impact of anthropogenic sound on the marine environment for environmental compliance of human-related activities.

Passive acoustic monitoring of the oceanic environment can be used as a tool to address this issue (Hildebrand, 2009). In recent decades, long-term passive acoustic monitoring systems were mainly allowing for (1) a description of the temporal and spectral properties, (2) a classification and (3) a quantification of the temporal presence or absence of natural and anthropogenic sounds usually received by a single omni-directional hydrophone [e.g. (Wiggins and Hildebrand, 2007)]. Due to recent advances in data acquisition technology, long-term passive acoustic recording systems are now able to sample data at much higher sampling frequencies ($\geq 100\,kHz$) from an array of hydrophones allowing tracking of low and high-frequency sounds in space and time [e.g. (Wiggins et al., 2012)].

In this PhD dissertation, techniques for passive acoustic tracking in all three spatial dimensions of both biological and anthropogenic sounds are developed for long-term acoustic datasets recorded continuously over months using custom-designed hydrophone arrays with spacing ranging from meters to kilometers. While in chapter 2 passive acoustic tracking methods are developed for shallow-diving toothed whales (e.g. killer whales) in the acoustically refractive environment of the upper ocean ($< 200\,m$), in chapter 3 small-aperture hydrophone arrays were embedded into a large aperture seafloor array to track the highly directional sounds of deep-diving ($< 1\,km$) toothed whales, such as Cuvier's beaked whales. These techniques allow to study their natural underwater movements and behavior as well as responses to anthropogenic sounds. For example,

(Henderson et al., 2014), investigated the impact of mid-frequency active SONAR sounds emitted during naval training exercises on delphinids by combining a variation of the acoustic tracking method developed in chaper 2 with visual observations. Besides behavioral studies, these tracking techniques have the potential to enhance the current passive acoustic abundance estimation of marine mammals by investigating the acoustical properties of marine mammal sounds such as sound intensity and directionality as exemplified for Cuvier's beaked whales in chapter 3. In chapter 4, an opportunistic method for a single-instrument deployment is introduced to track and measure the underwater radiated sound from ships, which is the dominating anthropogenic contribution to the underwater acoustic soundscape at low frequencies ($10 - 500\,Hz$).

Chapter 2

Offshore killer whale tracking using multiple hydrophone arrays

2.1 Abstract

To study delphinid near surface movements and behavior, two L-shaped hydrophone arrays and one vertical hydrophone line array were deployed at shallow depths ($< 125\,m$) from the floating instrument platform R/P FLIP, moored northwest of San Clemente Island in the Southern California Bight. A three-dimensional propagation-model based passive acoustic tracking method was developed and used to track a group of five offshore killer whales (Orcinus orca) using their emitted clicks. In addition, killer whale pulsed calls and high-frequency modulated (HFM) signals were localized using other standard techniques. Based on these tracks sound source levels for the killer whales were estimated. The peak to peak source levels for echolocation clicks vary between $170-205\,dB\,re\,1\,\mu Pa\,@\,1\,m$, for HFM calls between $185-193\,dB\,re\,1\,\mu Pa\,@\,1\,m$, and for pulsed calls between $146-158\,dB\,re\,1\,\mu Pa\,@\,1\,m$.

2.2 Introduction

Tracking odontocetes using acoustic arrays can provide insight into their abundance and submerged behavior. The use of towed hydrophone arrays for line transect

surveys has become an accepted method for abundance estimation of sperm whales [(Barlow and Taylor, 2005); (Lewis et al., 2007)], or to study their submerged behavior (Thode, 2005). The towed array is used to determine the bearing to vocalizing animals; their range is often estimated by observing their change in bearing as the tow ship moves past the animals' location. An alternative for detailed localization is to use vector sensors to provide directional information from multiple array elements (Thode et al., 2010), or to exploit multipath arrivals and interaction with range-dependent bathymetry (Tiemann et al., 2006). Likewise, widely-spaced (km-scale) seafloor arrays have been used to track sperm whales using their intense echolocation clicks [e.g., (Nosal and Frazer, 2007)]. However, smaller cetaceans, such as delphinids, produce echolocation clicks at higher frequencies that attenuate quickly over distance. Since their clicks are highly directional, the same click is often not detected at multiple elements within a km-scale array. To track clicks from small cetaceans, a smaller aperture array is needed [e.g., (Wiggins et al., 2012)].

In this paper, we describe a three-dimensional, propagation model-based tracking method which utilizes three small-aperture (meter-scaled) arrays deployed at shallow depths from the stationary Floating Instrument Platform (FLIP) (Fisher and Spiess, 1963). The capabilities of this method are illustrated by tracking a group of five clicking offshore killer whales (Orcinus orca) over a horizontal range of several hundred meters at shallow depths $(< 40\ m)$ in the refractive ocean environment of the Southern California Bight.

In addition to the impulsive, broad-band echolocation clicks used for foraging (Au et al., 2004), killer whales produce pulsed calls and frequency-modulated whistles for communicative purposes (Ford, 1989) as well as high-frequency modulated (HFM) calls with frequencies well above the typical whistle frequency range [(Samarra et al., 2010); (Simonis et al., 2012)]. To provide a more complete representation of the killer whales' paths and acoustic behavior, their HFM and pulsed calls were localized using

arrays of hydrophones separated by tens of meters and by a few kilometers, respectively.

2.3 Methods

2.3.1 Experimental setup

The research platform FLIP was placed in a nearly-stationary three-point mooring 7 km northwest of San Clemente Island in the Southern California Bight for 25 days during October and November 2008 (Figure 2.1). FLIP provides a stable observation deck 25 m above the sea surface from which visual observers can monitor cetaceans as they surface to breathe, in addition to providing a persistent platform for deploying instrumentation such as hydrophone arrays for acoustic monitoring. Deployed from FLIP to record marine mammal sounds for tracking were three small aperture hydrophone arrays: two L-shaped arrays (L1 and L2) each with one vertical leg and one horizontal leg at 36 m depth, and one Vertical Line Array (VLA) below the draft of FLIP at 122 m depth (Figure 2.2). Combining either L1 or L2 with VLA provides a medium aperture array with 86 m sensor spacing allowing signals with longer durations than clicks to be localized. L1 and L2 were separated horizontally by 12 m and were 12 m from the hull of FLIP (three times the hull diameter) with a 5° bearing for the horizontal leg of L1 and 60° bearing for the horizontal leg of L2, relative to FLIP face. This configuration reduces the shadowing from the hull of FLIP while enabling unambiguous locations of sound sources near the sea surface. The small-aperture hydrophone spacing of L1 and L2 are designed to be minimally redundant with spacings between 0.2 m and 2.15 m, to process low and high-frequencies with a small number of hydrophones. The spacing of the VLA arrays elements is 1.2 m. All three arrays were constructed from omni-directional spherical hydrophones (HS-150 Sonar Research and Development Ltd., Beverley UK) with a flat sensitivity ($\pm 2\ dB$) of $-205\ dB\ re\ V/\mu Pa$ from 1 kHz to 125 kHz. The 14 hydrophone

signals were band-pass filtered from 2 to 96 kHz and amplified using 14 separate circuit boards, which where custom-designed and built. Each signal was sampled continuously at 192 kHz with 16 bit resolution using two 8-channel Analog Digital Converters (ADC) (MOTU 896 - Cambridge, MA). The GPS (global positioning system) derived analog time code IRIG-B was sampled by one channel of both ADCs for time-synchronization. Each ADC was connected to a data acquisition computer streaming the 8 digitized channels into WAVE files and stored onto hard disks continuously resulting in 15 terabytes of data recorded during the 25 day deployment.

To characterize the refractive ocean environment, daily sound velocity profiles based on temperature, pressure and salinity (Chen and Millero, 1977) were obtained from deployments of a Seabird 29 CTD probe from FLIP.

A large aperture hydrophone array, consisting of four High-Frequency Acoustic Recording Packages (HARPs), was deployed near the seafloor (300 to 400 m depth) approximately 1 km north, east, south and west of FLIP (Figure 2.1). The four HARPs were each equipped with a single hydrophone, low-drift (10^{-8}) synchronized clocks, and recorded continuously at a sampling frequency of 200 kHz (Wiggins and Hildebrand, 2007).

2.3.2 Acoustic identification of killer whale sounds

The echolocation clicks and pulsed calls of killer whales have distinct characteristics, which together enable the discrimination to species level [(Barrett-Lennard et al., 1996); (Au et al., 2004)]. The killer whale sounds recorded during this experiment were identified as the non-mammal eating offshore ecotype by an expert of killer whale sounds (personal communications John Ford, University of British Columbia). However, no visual confirmation was possible since the killer whales passed by FLIP during night time. In addition, whistles could not be unambiguously distinguished from pulsed calls,

so these types of sounds were all considered pulsed calls.

2.3.3 Three-dimensional click localization

Impulsive, broad-band echolocation clicks were automatically detected in the recordings using a Teager energy detector on one channel of each array. Briefly, the Teager (Kaiser, 1990), or Teager-Kaiser energy, is a nearly instantaneous energy measurement whose discrete form can be computed from three samples. Teager energy responds rapidly to energy onset and was first proposed for marine mammal echolocation click detection by (Kandia and Stylianou, 2006). An independent implementation (Roch et al., 2011) detects clicks based on thresholds derived from order statistics and uses a region growing procedure e.g. similar to (Fristrup and Watkins, 1992) to find the start and end of each echolocation click. Further details may be found in (Roch et al., 2011). Vertical and horizontal angles were estimated from the vertical and horizontal hydrophones of the arrays using a Time Difference Of Arrival (TDOA) method as described below. Based on the TDOA obtained angles of the 3 arrays, range, depth and bearing were computed and then transformed to a click location in a Cartesian coordinate system with FLIP as the center. The clicks were evaluated by an analyst and associated with a single track or excluded as outliers.

The localization algorithms and the orientation of L1 and L2 were verified by tracking the propulsion noise of a ship at known GPS positions approximately $350-500\,m$ away with a horizontal bearing root-mean-square (rms) error of 3° and a range and depth rms error of 38 m and 21 m, respectively.

2.3.4 TDOA angle estimation

The broad-band echolocation clicks of delphinid species have an autocorrelation function with a highly pronounced peak and low side lobes due to their impulsive

character in the time domain (Au et al., 2004). Therefore, the TDOA (Δt) of a click recorded on any two hydrophones can be computed by cross-correlating the time series. For a delphinid high-frequency click produced several hydrophone spacing away from the two hydrophones, a plane wave approximation can be used (Figure 2.3). If the hydrophone spacing is d and the sound speed of the water is c, then the incident angle of the plane wave is:

$$\beta = \cos^{-1}\left(\frac{c \cdot \Delta t}{d}\right) \tag{2.1}$$

2.3.5 Range and depth

High-frequency clicks can be described as rays propagating in the refractive ocean environment characterized by a sound speed profile (Figure 2.4). For each click, the TDOA-obtained vertical angles from the VLA at 122 m depth and from the vertical leg (hydrophone 1 and 3) of L2 at 36 m were used as start angles for two rays, which were then back-propagated in the range-depth space using the BELLHOP propagation model (Porter and Bucker, 1987). The intersection of the rays yields a unique depth and range estimate for each click by finding the range-depth pair of each ray with the smallest difference to each other, using the non-linear minimization algorithm Nelder-Mead Simplex (Lagarias et al., 1998).

Due to the high sensitivity of the vertical angles, especially at large ranges for L1 and L2 (1.7° difference for a range change from 400 m to 300 m), the range and depth time series for tracked animals were smoothed using polynomials of the order 5 through 10.

Only the hydrophone pair 2-3 for L1 and 1-3 for L2 were used to obtain vertical angles due to temporarily and permanently malfunctioning hydrophones and significant differences in the noise levels between the hydrophones. Each of those hydrophone

combinations represent the best possible mix of low noise floors and large apertures (high TDOA sensitivity) for each of the legs. However, for the range and depth estimation the vertical leg of L1 was not used because it has a smaller aperture and significantly higher noise levels than the vertical leg of L2.

2.3.6 Bearing

Using the TDOA method and equation 2.1, angles to the clicks are estimated using the horizontal components of L1 and L2 respectively (Figure 2.5). Hydrophone pairs 5-6 for L1 and 4-6 for L2 were used to obtain bearings. These angles are mapped to horizontal bearings to account for the bias resulting from animal locations that are above or below the depth of the horizontal leg of L1 and L2. With the vertical angle β_{ver} obtained from the vertical component for a click and the direction cosines, the angle from the horizontal component β_{hor} can be mapped to a horizontal bearing β'_{hor}:

$$\beta'_{hor} = \tan^{-1}\left[\frac{\cos(\beta_{ver})}{1-[\cos(\beta_{ver})+\cos(\beta_{hor})]}\right] \tag{2.2}$$

With the known orientation of the horizontal component of L1 and L2, the horizontal bearing β'_{hor} can be converted into a bearing with a scale ranging from 0°(North) over 180°(South) to 360°(North) with respect to FLIP.

Due to the left-right ambiguity typical of line arrays, each horizontal component of L1 and L2 provides a set of two possible bearings (Figure 2.5). Since the clicking animals are typically much farther away than several times the distance between L1 and L2, crossing the bearings will give inaccurate locations. However, one of the bearings from L2 will line up with one of the bearings from L1 providing an unambiguous bearing to the sound source (Figure 2.5).

2.3.7 Associating pulsed calls with individual killer whales

The pulsed calls of the killer whales have a lower Signal-to-Noise Ratio (SNR) than the clicks and are longer in duration (several hundred milliseconds), which leads to an insufficient time resolution of the TDOA for the spacing of the three individual arrays with a maximal possible TDOA of 1 *ms*. This makes it difficult to localize them. However, since L2 and VLA are 86 *m* apart, the pulsed calls were cross-correlated between these two arrays to provide a sufficient TDOA time resolution. In addition, the localized clicks (subsection 2.3.1) of each killer whale are also cross-correlated between L2 and the VLA, yielding one set of click TDOAs for each of the five killer whales Then, the TDOA of a pulsed call at a given time is compared to the click TDOAs of each of the 5 killer whales around that time to associate the pulsed call with one of the 5 killer whales. If the difference between that pulsed call TDOA and the click TDOAs of a killer whale is smaller than 3 *ms* and the TDOA differences to all other killer whales are greater than 6 *ms*, a pulsed call is considered to be unambiguously associated with a particular killer whale track. For that reason, the location of the pulsed call is approximated by the location of a click produced by the associated killer whale at about the time of the pulsed call. This procedure eliminates the need to localize pulsed calls on the individual small aperture arrays and would also work for whistles since their duration is similar to the pulsed calls.

2.3.8 Localizing high-frequency modulated calls

The HFM signals occur during times when no click tracks are available and therefore the method in the previous section is not applicable. However, the HFM calls were recorded on the four seafloor HARPs and on the FLIP arrays, which form a large aperture array with spacing ranging from one to two kilometers. The TDOAs of the HFM calls between the HARPs and FLIP were manually picked. The three-dimensional localization

was conducted using the hyperbolic fixing algorithm (Spiesberger and Fristrup, 1990) assuming a constant sound speed profile. Since the rays travel rather straight paths due to greater vertical angles resulting from $300-400\,m$ depth difference between the HARPs and the killer whales, in contrast to $0-40\,m$ depth difference between L1 / L2 and the killer whales, refraction effects therefore were neglected for the large aperture seafloor array.

2.3.9 Source levels

Peak to peak source levels for each localized click, pulsed and HFM call were calculated from the sum of the peak to peak received level (RL_{pp}) and the transmission loss (TL). We assume spherical spreading, since the ranges to the killer whales, (r) are typically less than the water depth. We also include a frequency dependent attenuation coefficient (α). The TL is combined with the RL_{pp} to estimate the peak to peak Source Level (SL_{pp}) in $dB\ re\ 1\mu Pa$ @ $1\ m$ from:

$$SL_{pp} = RL_{pp} + 20\log_{10}(r[m]) + \alpha * r[m]/1000 \tag{2.3}$$

where α is taken to be $3\ dBkm^{-1}$ at $20\ kHz$ for the clicks and $5\ dBkm^{-1}$ at $25\ kHz$ for the HFM calls (Ainslie and McColm, 1998). The frequency attenuation term is neglected for the pulsed calls due to the low attenuation at frequencies below $10\ kHz$.

The peak to peak received level in $dB\ re\ 1\ \mu Pa$ of each killer whale sound is calculated from the maximum and minimum of its bandpass-filtered calibrated pressure time series $p(t)$ recorded by the L2 array hydrophone #4 using the reference pressure p_0 of $1\ \mu Pa$:

$$RL_{pp} = 10\log_{10}\left(\frac{Max\{p(t)\} + |Min\{p(t)\}|}{p_0}\right)^2 \tag{2.4}$$

Calibrations of the FLIP arrays and HARPs hydrophone sensitivities were performed at the U.S. Navy's Transducer Evaluation Center facility in San Diego, California and at the Scripps Whale Acoustics Laboratory at the University of California, San Diego.

2.4 Results

Approximately one hour after sunset on 11 November 2008, a group of five killer whales were tracked using their emitted sounds and the algorithms described above. Their echolocation clicks were short duration ($< 250\ \mu s$) signals with peak energy in the $10 - 30\ kHz$ band. These clicks showed variations on short time scales that may result from beampattern effects, with higher amplitude and higher bandwidth clicks assumed to be more nearly received on-axis [Figure 2.6 (a) and (b)]. HFM signals were moderate duration ($\approx 90\ ms$) frequency modulated downswept signals around 20 kHz with visible harmonics [Figure 2.6 (c)]. Pulsed calls were long duration ($\approx 0.5\ s$) rapidly modulated tones often with both side-banding and harmonics (Figure 2.7).

Detailed bearings, ranges and depths of the echolocation clicks fall along discrete tracks over a period of about 5 minutes. A single track is shown in Figure 2.8; individual range and depth estimates are fitted with polynomials to aid with interpretation. The peak to peak source level estimates of the clicks [Figure 2.8 (d)] vary between 170 and 205 $dB\ re\ 1\ \mu Pa\ @\ 1\ m$, in good agreement with previous estimates (Simon et al., 2007), but about 20 dB lower than what has been reported for Northeast Pacific resident killer whales (Au et al., 2004).

Three-dimensional tracks for five killer whales were estimated using over 700 clicks, 9 pulsed calls and four HFM calls from about an eight minute period (Figure 2.9). Individuals from the group were first localized about 350 m east to southeast of FLIP heading northwest. Killer whales A and B transit south of FLIP, while killer whales C, D and E travel east of FLIP. As all of the killer whales get closer to FLIP, they decrease

their depth from about 40 m to less than 5 m when they reach their closest point of approach (CPA) to FLIP. The minimum distance of the killer whales to FLIP was always greater than 100 m. The durations of the killer whale tracks vary between two to five minutes. Around 02:43:41 GMT, the tracks of killer whales A and B appear to merge into one track, leaving it unclear whether the track belongs to killer whale A or B or both. The magnitude of the velocity vector of the killer whales varies between 1 kmh^{-1} and 10 kmh^{-1}. When passing FLIP, whales C and A/ B slow down temporarily from 6 kmh^{-1} to 2 kmh^{-1}, while whales D and E travel at average speeds of 9 kmh^{-1} and 5 kmh^{-1}, respectively.

The HFM calls were localized approximately 500 m northwest of FLIP with peak to peak source level estimates ranging between 185 and 193 $dB\ re\ 1\ \mu Pa\ @\ 1\ m$ [Figure 2.6 (c)]. These locations further suggest the overall northwest movement of the killer whale group.

The peak to peak source levels of the last pulsed call from the killer whales A, B, C and D in Figure 2.9 were 146, 153, 158 and 150 $dB\ re\ 1\ \mu Pa\ @\ 1\ m$, respectively (Figure 2.7). Although there are variations in the degree of frequency modulation, number of harmonics and call length, no characteristics to distinguish individuals could be established due to the limited number of pulsed calls per track (Figure 2.9).

2.5 Discussion

The accuracy of the killer whale sound localizations depends on the knowledge of the array element locations, the accuracy of the calculated TDOA based on the time-bandwidth product of each killer whale sound type and the knowledge of the sound velocity field.

Although the inter-element spacing of each of the arrays are known with an accuracy of less than one centimeter and the array orientation was calibrated by tracking

ship noise from known GPS locations, L1 and L2 potentially could be vertically inclined and horizontally rotated by an unknown small angle due to their mounting configuration and ocean currents leading to increased uncertainty in vertical angles and bearings. Equipping the arrays with a compass and a tilt sensor would help to monitor the array orientations in future deployments. In addition, the vertical components of L2 and the VLA used for the range and depth estimation were not vertically aligned and were off-axis by less than 10 m, which contributes to the uncertainty of the range and depth estimates for the clicks by less than 5 m respectively.

The hydrophone spacing of L1, L2 and VLA provides maximum TDOAs around 1 ms allowing clicks, which are typically short duration ($< 250\ \mu s$), to be used for angle estimates with errors smaller than 2°. However, all other killer whale sounds (HFM and pulsed calls) have a comparably smaller bandwidth, lower SNR and longer duration than the clicks, preventing their being used for cross-correlation, which would result in large angle uncertainties. Therefore, a frequency-domain beamformer for L1 and L2 was investigated by splitting the L-shape up into two line arrays with three elements each or by utilizing the entire L-shape with all 6 hydrophones as a two-dimensional array to exploit the maximum possible array gain. In either case, the results were unsatisfactory since the wavelengths of the pulsed calls are too large for the array spacing and the bandwidth of the pulsed calls is usually too small to resolve the spatial aliasing by frequency averaging of the beamformer outputs (Thode et al., 2000). To overcome these limitations, the pulsed calls were cross-correlated between hydrophones of different arrays; for example, cross-correlating the signal from one hydrophone of L2 with one from VLA. Pulsed calls, which often overlap with clicks, were cross-correlated only during periods free of clicks to prevent contamination from the higher SNR of the clicks. Due to a varying SNR of the pulsed calls and occasionally similar click TDOAs for different animals around the same time instance, only a fraction of the pulsed calls could be confidently and ambiguously

associated with specific animals (9 out of 60 detected pulsed calls).

The location error of the HFM calls was about 150 m assuming 5 m uncertainty in the positions of FLIP and the four HARPs, 10 ms uncertainty in the TDOAs and 20 ms^{-1} uncertainty in the sound speed. However, the location errors of the HFM calls contribute less than 4 dB to their source level error because of the logarithmic relationship between TL and range at these distances with respect to FLIP ($\approx 500\ m$).

For the higher-resolution three-dimensional click localization method, a range and bearing independent sound speed field was assumed [Figure 2.4 (b)]. The sound speed profile was obtained just 8 h before the killer whale tracks. Depending on the sound speed profile, the array locations and the clicking killer whale locations, this method provides more accurate ranges and depths than simply intersecting straight lines starting with the TDOA measured angles of L2 and VLA. For example, for the measured sound speed profile [Figure 2.4 (a)] and a killer whale 264 m away at a depth of 19 m, the error of the location based on simply crossing the vertical angles is 30 m and 15 m for range and depth, respectively.

The scatter in the range and depth estimates from the clicks was greater than for the bearing estimates because of source and receiver geometry. For example, plane waves arriving nearly perpendicular to array components will have TDOAs that are more sensitive to changes in angle than waves arriving along the array axis because of the cosine relation in equation 2.1. This was the case for the vertical arrays when the killer whales were far away or at the array depth. A polynomial smoothing function for the range and depth estimates was chosen over a Kalman filter because it is easy to implement and provides clean large-scale tracks at the cost of averaging out possible fine-scale movements, i.e. possible 10 m up and down dive within 10 sec as shown in Figure 2.8 c. Testing if a particle or even a Kalman filter could separate out these fine-scale movements from the measurement noise, is a subject for further investigation.

Only a few surface or bottom reflections were found in the recordings, preventing multipath localization techniques from being used. Furthermore, the three-dimensional click localization method requires that the same killer whale click was received on all three arrays deployed from FLIP. After the killer whales passed FLIP, tracking was discontinued because the number of clicks on all arrays was significantly reduced. The shallow depths near the CPA suggest the whales were surfacing, perhaps to breathe, and therefore may have reduced their clicking rates. In addition, clicks are highly directional and after the closest-point-of-approach with FLIP, the headings of the click beams were no longer directed toward the arrays.

The estimated click peak to peak source levels vary between 170 and 205 dB re 1 μPa @ 1 m probably because of the click beam pattern and the orientation of the killer whale with respect to the array (L2). For example, the source level rose and fell by about 20 dB over short periods suggesting the click beam angle was swept through the array direction [Figure 2.8 (d)] rather than caused by location error, since the logarithmic relationship between transmission loss and range limits the error in source level to less than 3 dB. Therefore, the near on-axis and off-axis clicks in Figure 2.6 (a) and (b) were recruited from killer whale C as it is assumed to increasingly point its acoustic beam towards array L2 with a maximum SL_{pp} of 202 dB re 1 μPa @ 1 m (considered to be near-on axis) and then away from the array with a minimum SL_{pp} of 181 dB re 1 μPa @ 1 m (considered to be off-axis) between 02:43:00 GMT and 02:43:16 GMT [Figure 2.8 (d)]. The decrease of energy at higher frequencies (> 40 kHz) for the off-axis click [Figure 2.6 (b)] compared to the near on-axis click [Figure 2.6 (a)] is another suggestion for directionality of these clicks. The consistent multipath arrivals for the near on-axis and off-axis clicks, which are identical across all channels of array L2, suggests that they are not caused by the arrays and but instead might be created by the sound production mechanism of the killer whale itself, as described for other clicking toothed whales

(Cranford, 2011).

2.6 Conclusions

A three-dimensional propagation-model based passive acoustic tracking method for broadband echolocation clicks was developed for two L-shaped arrays and one vertical line array deployed from FLIP. Using these small aperture arrays together with the medium-aperture array from L2 to VLA and the large aperture between the FLIP arrays and the 4 HARPs around FLIP, a group of five offshore killer whales was tracked by using their emitted clicks as well as their pulsed and HFM calls. Based on the tracks, the speed of each killer whale and the source levels for all three call types were estimated.

These acoustic methods provide a tool to track and study other delphinid species. If conducted during daylight hours, the acoustic tracks and behaviors also can be compared with the visually observed surface behaviors to provide a more comprehensive understanding of their habitat use than by either technique individually.

2.7 Acknowledgments

Funding for this research was provided by the U.S. Navy CNO-N45 and the Naval Postgraduate School; we thank Frank Stone, Ernie Young, Curt Collins, and John Joseph for support and assistance. We thank the Scripps Whale Acoustics Lab members, especially Ethan Roth, Chris Garsha, and Brent Hurley for help with data collection as well as Bill Hodkgiss and Greg Campbell for useful discussions. Furthermore, we thank the FLIP crew members, particularly Bill Gaines, Captain Tom Golfinos, Paul Porcioncula, and Greg Viehmann. We also thank Amalis Riera, Volker Deecke, and John Ford for their efforts in determining the killer whale ecotype.

Chapter 2, in full, is a reprint of the material as it appears in Gassmann, M., Henderson, E. E., Wiggins, S. M., Roch, M. A., and Hildebrand, J. A. (2013). Offshore killer

whale tracking using multiple hydrophone arrays. *The Journal of the Acoustical Society of America*, 134(5):35133521. The dissertation author was the primary investigator and author of this paper.

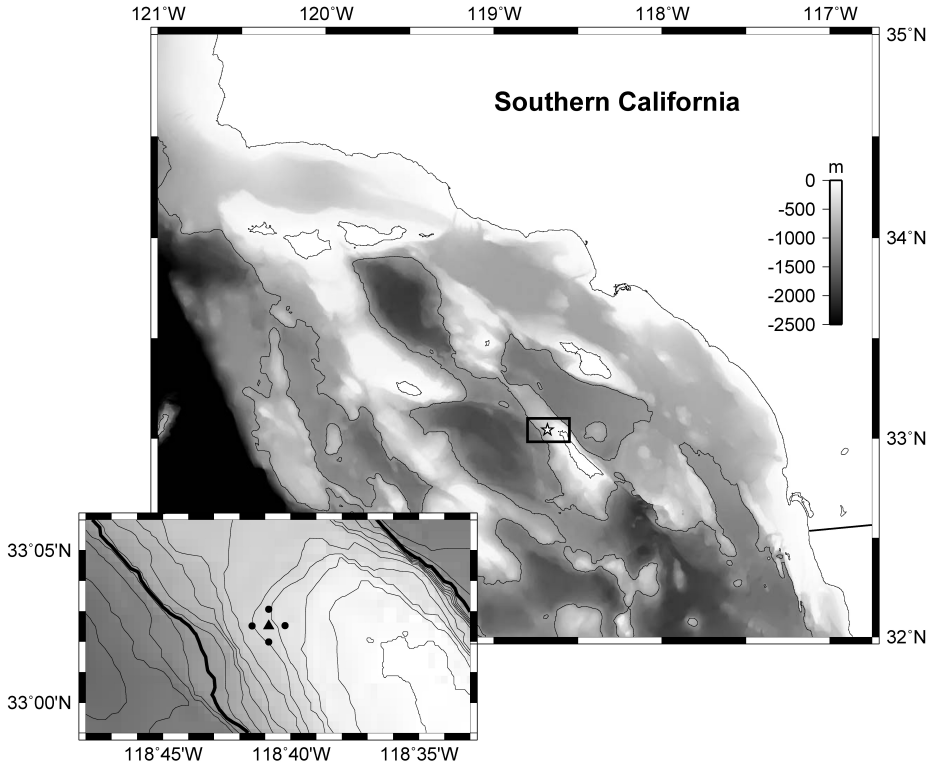

Figure 2.1. Location of FLIP (triangle) in the Southern California Bight northwest of San Clemente Island. Four HARPs (dots) are located 1 *km* north, east, south and west of FLIP on the seafloor at $300-400$ *m* depth. Bathymetry contours are every 200 *m* with the thick black contour at 1000 *m*.

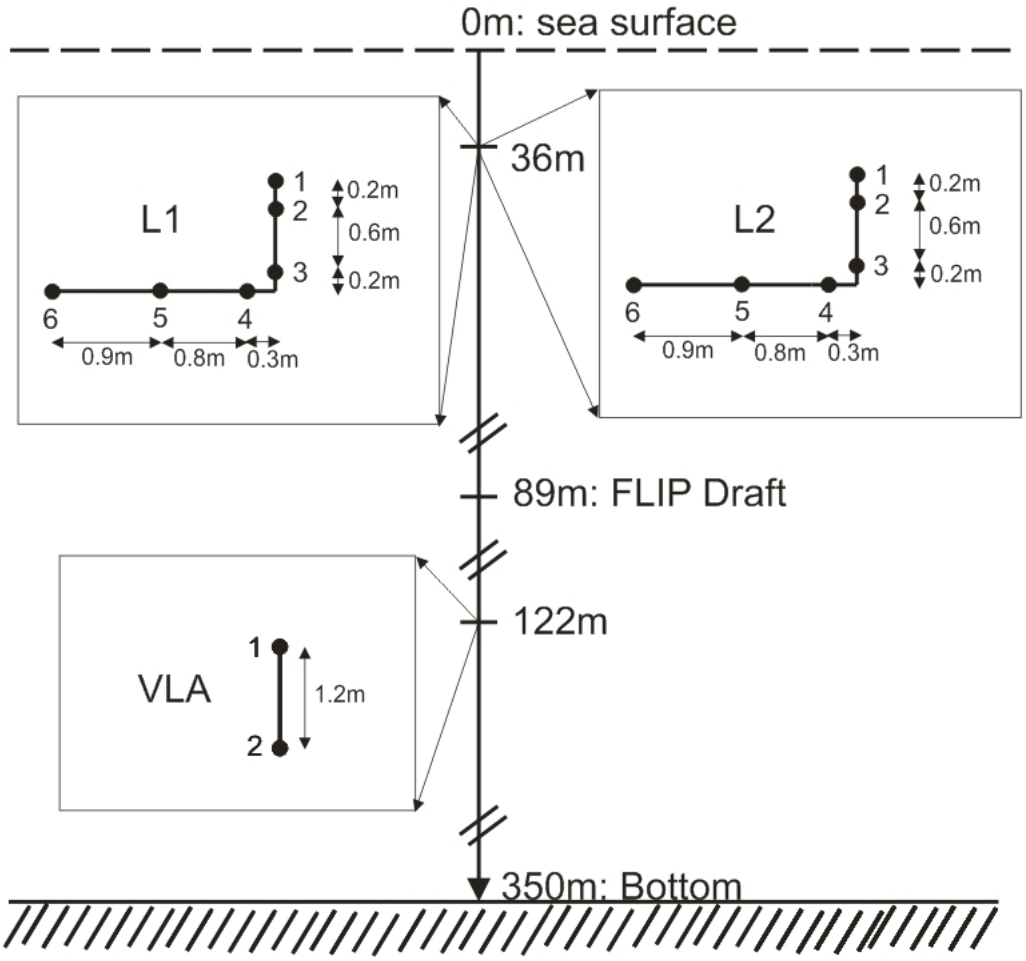

Figure 2.2. Hydrophone array configuration. The two L-shaped arrays L1 and L2 are located 36 *m* below the sea surface on the port and starboard-side of FLIP, respectively. The Vertical Line Array (VLA) is located 86 *m* below the L-shaped arrays at 122 *m* depth.

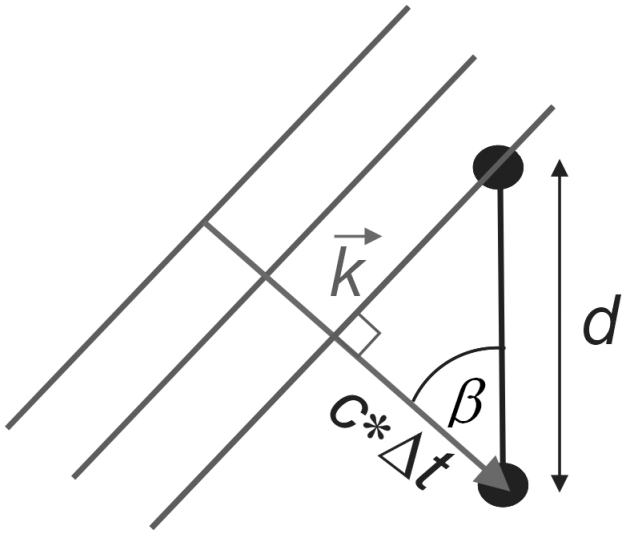

Figure 2.3. Measurement of the Time Difference Of Arrival (TDOA). The angle, β, of an incoming plane wave with wave number vector, $\vec{k}$, is the inverse cosine of the TDOA, Δt, and the speed of sound, c, divided by the distance between the two sensors, d, (see equation 2.1).

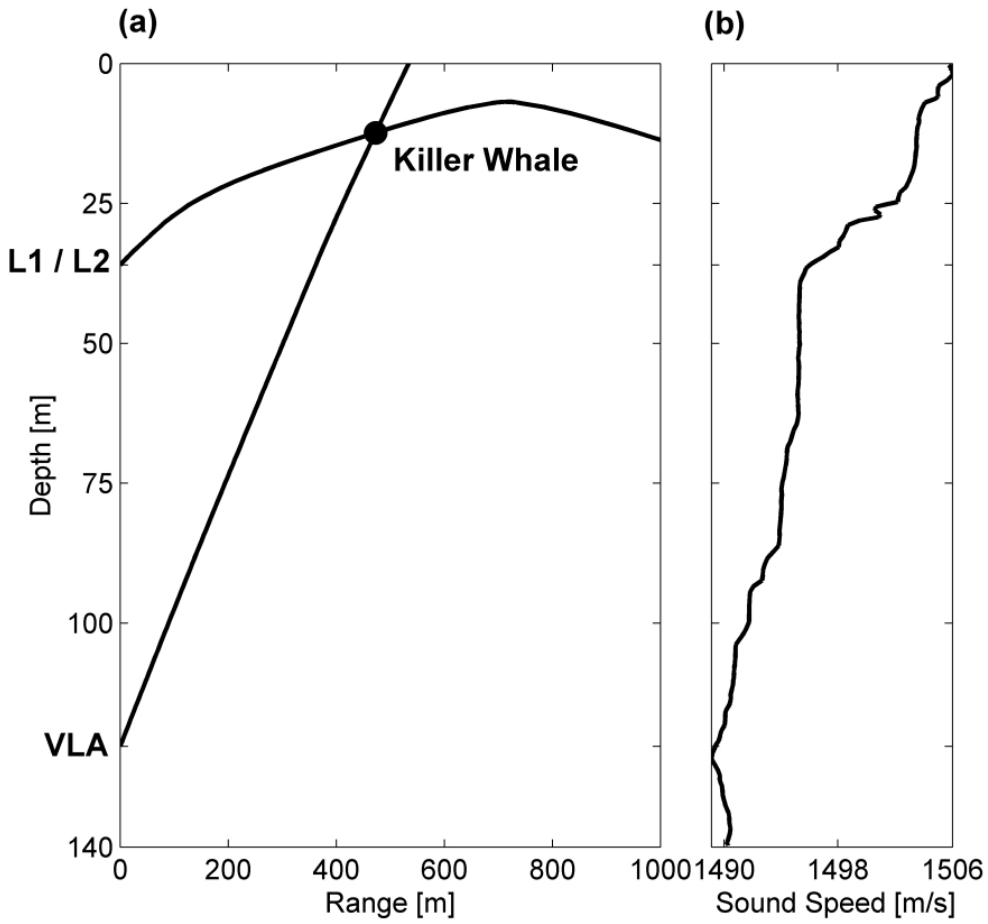

Figure 2.4. Range and depth estimation. Intersection of rays (a) provides a range and depth estimate for a clicking killer whale (black circle). The vertical arrival angles at the L-shaped arrays and VLA were used as start angles for two rays, which were back-propagated using the measured sound velocity profile (b) to account for refraction.

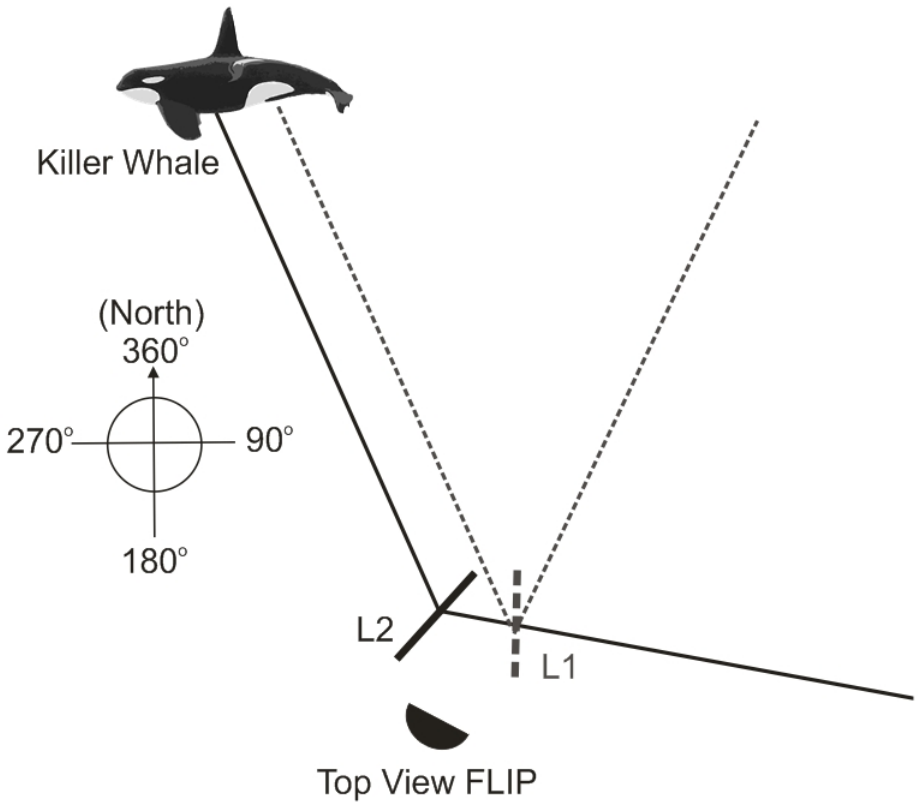

Figure 2.5. Bearing estimation. Bearings of the horizontal components for the L1 and L2 arrays are represented by the dashed line and the solid line, respectively. Each array measures two possible bearings due to the left-right ambiguity common to line arrays. This ambiguity is resolved by selecting the bearings that give consistent locations between L1 and L2.

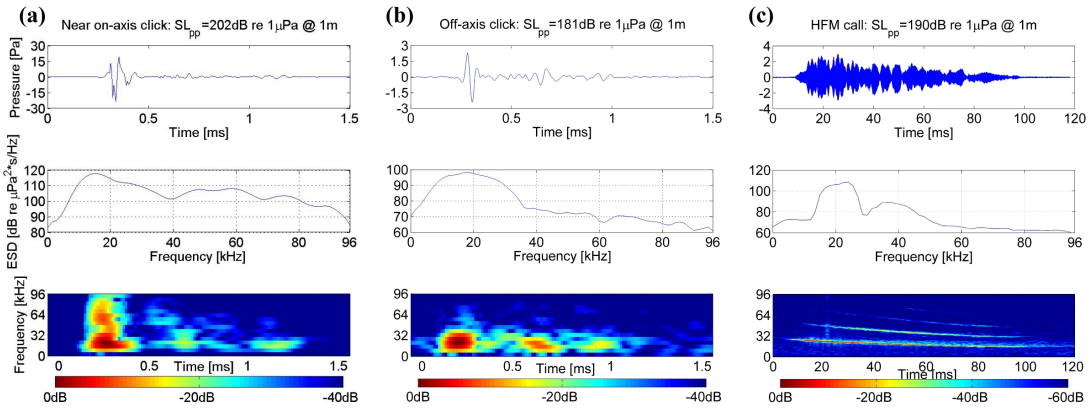

Figure 2.6. Pressure time series, normalized spectral densities and spectrograms of a received near on-axis click (a), an off-axis click (b), and an HFM call (c). Peak to peak source levels (SL_{pp}) are obtained from the pressure time series using equation 2.3. Spectrograms were calculated with Hamming windows, 32 and 512 sample FFTs with 95% overlap for the clicks and HFM call, respectively. Spectrograms and spectral densities were normalized by their maxima. Both clicks in (a) and (b) are about 250 μs long and have two multipath arrivals about 0.5 *ms* and 0.8 *ms* after the first arrival. The HFM call in (c) is a frequency modulated downsweep around 20 kHz with 3 harmonics.

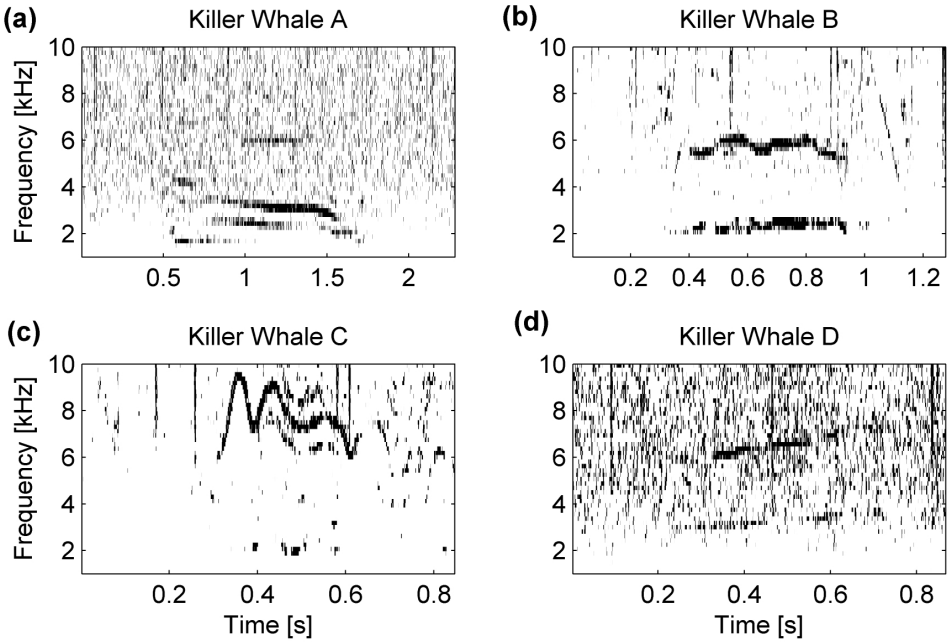

Figure 2.7. Spectrograms for the last localized pulsed calls for the killer whale tracks A (a), B (b), C (c) and D (d) (see Figure 2.9). Spectrograms were computed with 512 sample FFTs with 90% overlap using Hamming windows.

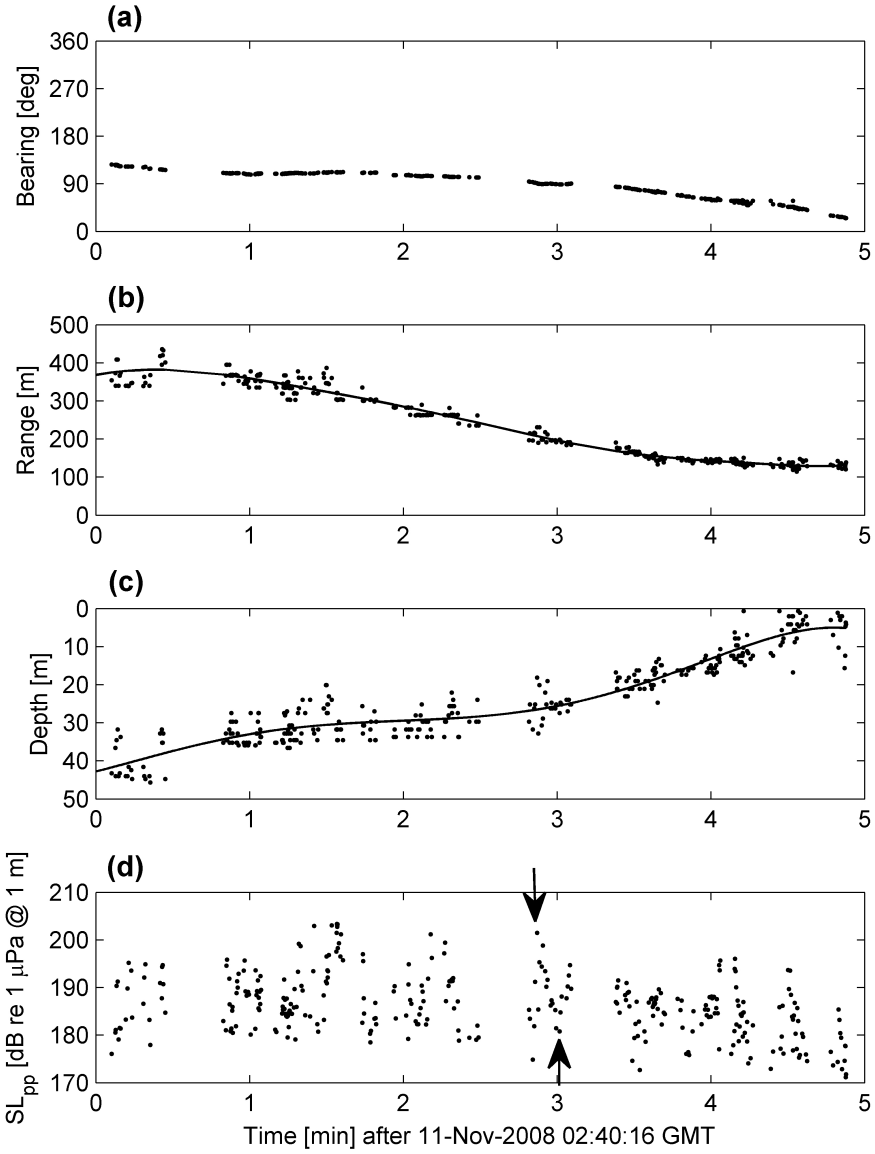

Figure 2.8. Bearings (a), ranges (b), depths (c), and peak to peak source level (d) estimates for the click track from killer whale C. Ranges and depths were smoothed with polynomial functions represented by the solid lines in (b) and (c). The down and upward pointing arrow in (d) around the 3^{rd} minute highlights the clicks used in Figure 2.6 (a) and (b) as a near on-axis and off-axis click respectively.

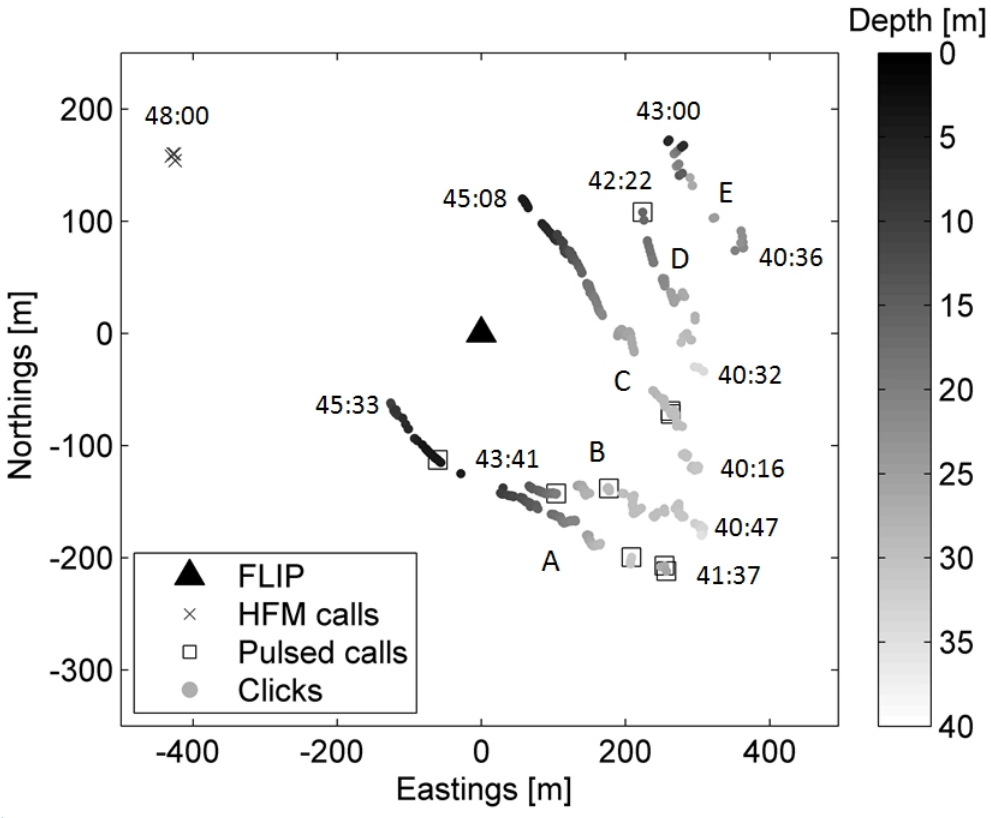

Figure 2.9. Three-dimensional tracks of the killer whales A, B, C, D and E relative to FLIP. Depths of click localizations are represented by the greyscale bar on the right. Boxes indicate pulsed calls. High-frequency modulated (HFM) call localizations are shown as cross marks. Times are in minute-second format (mm:ss) after 2008-11-11 02:00:00 GMT.

Chapter 3

Three-dimensional tracking of Cuvier's beaked whales' echolocation sounds using nested hydrophone arrays

3.1 Abstract

Cuvier's beaked whales (Ziphius cavirostris) were tracked using two volumetric small-aperture (≈ 1 *m* element spacing) hydrophone arrays, embedded into a large-aperture (≈ 1 *km* element spacing) seafloor hydrophone array of five nodes. This array design can reduce the minimum number of nodes that are needed to record the arrival of a strongly directional echolocation sound from five to two, while providing enough time-differences of arrivals for a three-dimensional localization without depending on any additional information such as multi-path arrivals.

To illustrate the capabilities of this technique, six encounters of up to three Cuvier's beaked whales were tracked over a two-month recording period within an area of 20 km^2 in the Southern California Bight. Encounter periods ranged from 11 *min* to 33 *min*. Cuvier's beaked whales were found to reduce the time interval between echolocation clicks while alternating between two inter-click-interval regimes during

their descent towards the seafloor. Maximum peak-to-peak source levels of 179 and 224 $dB\ re\ 1\ \mu Pa\ @\ 1\ m$ were estimated for buzz sounds and on-axis echolocation clicks (directivity index = 30 dB), respectively. Source energy spectra of the on-axis clicks show significant frequency components between $70-90\ kHz$, in addition to their typically noted FM upsweep at $40-60\ kHz$.

3.2 Introduction

Animal tracking can be used to study their migration, behavior, abundance and responses to man-made influences. Current tracking methods for marine mammals include visual observations, attaching small tracking devices (”tags”) to them, and passive acoustic monitoring that utilizes their emitted sounds. Visual tracking is difficult for deep-diving marine mammals, such as beaked whales, which are most often submerged below the sea surface. It is possible to attach tags to beaked whales, for example, short-term ($\approx 24\ h$) suction-cup archival tags to provide high-resolution depth profiles along with wide bandwidth recorded sound (Tyack et al., 2006), but it is difficult to infer detailed horizontal movement patterns and their position relative to local seafloor depths from these data. In contrast, barb-attached satellite tags provide large-scale horizontal movement patterns for up to a several months, but the resolution of their movements is coarse, as satellite-based locations are estimated only several times per day when the whale is at the surface (Schorr et al., 2014). Independent of the type of tag used, their attachment may alter the beaked whales' behavior and it is usually challenging to attach them, limiting the number of tagged individuals.

Passive acoustic tracking methods can be applied to toothed whales by localizing their repeatedly transmitted echolocation pulses with hydrophone arrays deployed near the sea surface. For example, three-dimensional tracking from a floating instrument platform has been demonstrated for killer whales that dive at shallow depths (Gassmann

et al., 2013), while for deep-diving beaked whales bearings were estimated from a towed hydrophone array (Yack et al., 2013). Although ranging with a towed hydrophone is possible, certain conditions on the geometry between the beaked whale and the towed array are required and limit its ranging capabilities (Zimmer, 2013).

Another approach to track deep-diving toothed whales is to use bottom-mounted hydrophones. For example, three-dimensional tracking has been demonstrated for a sperm whale by utilizing the arrival times of direct paths, surface and bottom reflections from its intense echolocation sounds recorded on a single, moored hydrophone (Tiemann et al., 2006). However, one of the limiting requirements of this multipath arrival technique is a seafloor that significantly varies horizontally around the hydrophone location. For tracking deep-diving sperm whales over any bathymetry, their echolocations sounds, although narrow beam, are intense enough in directions other than the main beam to be received on conventional seafloor arrays with the receivers spaced several kilometers apart. By computing a sufficient number of time-difference of arrivals (TDOAs) between receivers for each echolocation sound, three-dimensional trajectories of sperm whales can be reconstructed [e.g. (Nosal and Frazer, 2007)]. In contrast to sperm whales, it is more challenging to receive echolocation sounds of beaked whales on a sufficient number of kilometer-spaced receivers for three-dimensional tracking due to greater frequency absorption at their dominant frequencies ($> 10\ dB/km$) and lower source levels (Zimmer et al., 2005). To aid three-dimensional tracking of beaked whales with conventional seafloor hydrophone arrays in which receivers are spaced several kilometers apart, depth profiles of beaked whales recorded by time-synchronized suction-cup tags can be used to minimize the number of required receivers (Shaffer et al., 2013). However, the difficulty of attaching tags limits the number of individuals that can be tracked with this approach. To understand beaked whales' behavior and behavioral responses to man-made sounds (DeRuiter et al., 2013), horizontal movement patterns and their

corresponding depth profiles from a large number of tracked individuals would be beneficial. Passive acoustic tracking has the potential to better facilitate whale behavior and movement pattern studies if the required number of widely spaced receivers for a three-dimensional localization can be reduced without relying on depth information from suction-cup tags or multipath arrivals. In this paper, we address the beaked whale localization problem by introducing two volumetric hydrophone arrays with element spacing of approximately 1 *m* (Wiggins et al., 2012) into a conventional large-aperture seafloor array with a total of five nodes spaced up to 1 *km* apart. As a three-dimensional direction to an echolocating beaked whale can be estimated from each of the two small-aperture volumetric arrays, a three-dimensional location can be estimated by cross-fixing the two three-dimensional directions. This reduces the required number of widely spaced receivers to two for locations that are not collinear to the axis connecting the two volumetric arrays (Hirotsu et al., 2010). To take advantage of the entire five node seafloor array, a maximum likelihood estimator is implemented that utilizes all available arrival times of an echolocation sound at the two volumetric arrays and the three single-hydrophone receivers to estimate the three-dimensional location of a Cuvier's beaked whale (Ziphius cavirostris). To illustrate the capabilities of this technique, single Cuvier's beaked whales, as well as groups of up to three individuals, were tracked within an area of 20 km^2 in the Southern California Bight with track durations up to 33 *min*. A total of 11 tracks provide insight into the behavior of deep-diving Cuvier's beaked whales such as elevation above the local seafloor in addition to source level estimates for echolocation and buzz sounds.

3.3 Methods

3.3.1 Experimental setup

An array of five autonomous high-frequency acoustic recording packages (HARPs) with separations ranging from 406 to 1059 m was deployed on a seafloor slope in an area of known beaked whale habitat [Site N in (Baumann-Pickering et al., 2014) in the Southern California Bight (Figure 3.1 and Table 3.1]. While the center (C), eastern (E) and southern (S) HARPs were each equipped with a single hydrophone (Wiggins and Hildebrand, 2007), the northern (N) and western (W) HARPs were each equipped with a volumetric array of four hydrophones (Wiggins et al., 2012). The fixed array configuration was improved to reduce reflections from the support structure by mounting the four hydrophones at the top of fiber-glass masts. The hydrophone spacing ranged from 0.9 to 1.7 m with the top hydrophone (#1) being 3.5 m above the seafloor [Figure 3.2 (a) and (b)]. For all HARPs, hydrophone sensitivities and transfer function calibrations were performed at the Scripps Whale Acoustics Laboratory and at the U.S. Navy's Transducer Evaluation Center facility in San Diego, California. Minima of the HARPs' peak-to-peak clipping levels ranged from 158.5 to 159.8 $dB\ re\ 1\ \mu Pa$ at 42 kHz, which is close to the center frequency of Cuvier's beaked whale echolocation clicks.

Data were recorded continuously from December 2010 to February 2011 for 63 days at a sampling frequency of 200 kHz for the single sensor HARPs (C, E and S) and at a sampling frequency of 100 kHz for the four-channel HARPs (N and W). On January 6, 2011, HARPs E and S were refurbished and redeployed 118 and 76 m westwards from their initial location, respectively.

To compute harmonic mean sound speeds (Send et al., 1995) and to detect potential changes in the sound speed profile over the duration of the experiment, two full ocean depth conductivity, temperature, and depth (CTD) casts were conducted at

the location of HARPs E and N during the seafloor array deployment and recovery, respectively. Figure 3.3 shows the seafloor-to-bottom CTD cast from the recovery day and the corresponding sound velocity profile (Del Grosso, 1974). No significant change in sound speed ($> 1\ ms^{-1}$) below depths of 35 m between deployment and recovery CTDs was found. From the deployment and recovery sound speed profiles, time-independent harmonic mean sound speeds of 1484.7 and 1484.9 ms^{-1}, respectively, were computed for steep surface-to-bottom paths.

The HARP locations (Table 3.1) were estimated with a root-mean-square (rms) error of 4 m by applying a least-squares inverse to two-way travel times of pings travelling between a global positioning system (GPS)-located ship (R/V Sproul) and the acoustic release transponder of each HARP (Wiggins et al., 2013). The known distances between the acoustic release transponders and the hydrophones (3 to 12.5 m) yield the hydrophone depth estimates in Table 3.1. The time-invariant orientations of the static hydrophone arrays of HARPs N and W were obtained by cross-correlating the recorded broad-band ship noise from 150 GPS-referenced locations, which were horizontally distributed 360° around each HARP at a radius of less than the water depth, to minimize sound refraction effects caused by the depth-dependent sound speed profile. Using a spherical propagation model with a harmonic mean sound speed, c, for each ship location, $\mathbf{s}_{i,j,k} = (x_i, y_j, z_k)$, the predicted time-difference of arrival between two hydrophones p and q, with their location vectors $\mathbf{h}_p = (h_{px}, h_{py}, h_{pz})$ and $\mathbf{h}_q = (h_{qx}, h_{qy}, h_{qz})$, respectively, was obtained by

$$\mathbf{TDOA}_{\mathbf{pred}\ p,q} = \frac{\|\mathbf{h}_p - \mathbf{s}_{i,j,k}\| - \|\mathbf{h}_q - \mathbf{s}_{i,j,k}\|}{c}, \tag{3.1}$$

with $\|\cdot\|$ being the ℓ^2 norm, equation 3.1 yields a vector of the six predicted time-differences of arrival for each small-aperture array, $\mathbf{TDOA}_{\mathbf{pred}}$. The sum of the squared

differences between the predicted and cross-correlated time-differences of arrivals, $\mathbf{TDOA_{pred}}$ and $\mathbf{TDOA_{meas}}$, respectively, was minimized for all 150 ship locations to yield the hydrophone matrix, $\mathbf{H} = [\mathbf{h}_1, \mathbf{h}_2, \mathbf{h}_3, \mathbf{h}_4]$, which contains the Cartesian coordinates for each of the four hydrophones with respect to the geo-referenced acoustic transponder of each of the two HARPs with a small-aperture array:

$$min \left\{ \sum_i \sum_j \sum_k |\mathbf{TDOA_{pred}}[\mathbf{s}_{i,j,k}] - \mathbf{TDOA_{meas}}[\mathbf{s}_{i,j,k}]|^2 \right\} \rightarrow \mathbf{H} \, . \tag{3.2}$$

According to the hydrophone matrices, $\mathbf{H}$, the x axis of HARPs N and W, as defined in Figure 3.2 (b), was orientated at a bearing of 210° and 312°, respectively. There was no significant inclination of the x-y plane relative to the sea surface for the small-aperture arrays at N and W. The small-aperture array orientations were confirmed by estimating three-dimensional directions (Wiggins et al., 2012) to the three single-hydrophone HARPs (using their transponder reply pings), and to known ship GPS locations, with a rms error of less than 3°. To ensure clock synchronicity between the five HARPs, pings from the HARPs' acoustic transponders were emitted and received at each known HARP location at the beginning, after 27 days and at the end of the experiment in addition to measuring drift rates and offsets before and after the deployments with a high precision $(100\,ns)$ satellite-based clock (Wiggins et al., 2013). HARP clock drift rates were constant over the duration of the deployment, but varied across the HARPs between 8.8×10^{-10} (HARP C) and 2.8×10^{-9} (HARP N). This results in a total drift of 4.8 *ms* for HARP C and 15.2 *ms* for HARP N over the deployment of 63 days.

3.3.2 Acoustic detection and classification of Cuvier's beaked whale sounds

During their dives, Cuvier's beaked whales produce regular echolocation sounds, called clicks. The unique features of Cuvier's beaked whale click signals, throughout the

world's oceans and in particular in the Southern California Bight, have been previously described and hence enable unambiguous classification of this species (Baumann-Pickering et al., 2014). While start and end times of Cuvier's beaked whale dives were manually determined in long-term spectrograms of the acoustic data (Wiggins and Hildebrand, 2007), a Teager energy detector was used to detect the clicks automatically on each of the five HARPs (Roch et al., 2011). In addition to clicks, we observed other sounds such as rapid click trains, called buzzes (Johnson et al., 2004). If a localized buzz sound originates from near a Cuvier's beaked whale regular-click location and no other marine mammal species was acoustically present, it was considered with high confidence that the buzz was emitted by the regular-click localized Cuvier's beaked whale.

3.3.3 Three-dimensional localization

Click association and time-difference of arrival computation

Each detected click on any given HARP was associated with the clicks detected on the other four HARPs within a given time window to exclude click associations that exceed the maximum possible TDOAs between the five HARPs. The maximum possible TDOA for each of the 10 large-aperture hydrophone pair combinations ranged from 0.274 to 0.714 s and was computed as the quotient of the slant ranges between any two HARPs and the near-seafloor sound speed. Hence, the time windows for the four peripheral HARPs were centered at the click arrival time of the center reference HARP and had a maximum duration of the click duration plus two times the maximum possible time lag between the two HARPs on which the clicks were detected.

Ambiguous click associations can exist for groups of clicking beaked whales and for HARP pairs with maximum possible TDOAs greater than the beaked whales' inter-click-interval (ICI), especially since most clicks were not recorded by all five HARPs due to the echolocation click's beam directionality with a directivity index (DI) of 25 dB as

estimated by (Zimmer et al., 2005). Therefore, the TDOA of the associated clicks were computed and displayed for each HARP pair for an entire dive, yielding semi-continuous TDOA trajectories from which the ambiguities can be manually resolved. In contrast to the large-aperture array, no ambiguities in click associations for the small-aperture arrays needed to be resolved since a click was always received on all four hydrophones and the maximum possible TDOA was on the order of 1 *ms*.

TDOAs were computed from the peak of the cross-correlated times series between pairs of hydrophones. The total number of TDOAs depends on the number of HARPs that received a given click and ranged from 15 to 22 TDOAs. For instance, when a click is received on all five HARPs, 22 TDOAs were used: 6 TDOAs from each of small-aperture arrays, gathered in the vector $\mathbf{TDOA_{smlmeas}}$ and 10 TDOAs from the five-element large-aperture array (only hydrophone #1 is used from HARP N and W), gathered in the vector $\mathbf{TDOA_{lrgmeas}}$. We required that clicks were received on three or more HARPs and that small-aperture array HARPs were included in the solution, with 15 being the minimum number of TDOAs required for estimating a three-dimensional location.

Grid search algorithm

To find the location of the click-emitting beaked whale in Cartesian coordinates, $\mathbf{s_{Zc}} = (x_{Zc}, y_{Zc}, z_{Zc})$, a maximum likelihood estimator (Nosal and Frazer, 2007) was implemented that minimizes the sum of the squared differences of the measured ($\mathbf{TDOA_{smlmeas}}$ and $\mathbf{TDOA_{lrgmeas}}$) and the predicted ($\mathbf{TDOA_{smlpred}}$ and $\mathbf{TDOA_{lrgpred}}$) sets of time-differences of arrivals for the small and large-aperture arrays, for each source location candidate, $\mathbf{g}_{i,j,k} = (x_i, y_j, z_k)$, within the defined model space.

To compute the predicted $\mathbf{TDOA_{smlpred}}(\mathbf{g}_{i,j,k})$ and $\mathbf{TDOA_{lrgpred}}(\mathbf{g}_{i,j,k})$ at each grid point, $\mathbf{g}_{i,j,k}$, a spherical propagation model (equation 3.1) with a constant sound

speed of $c = 1484\ ms^{-1}$ was used due to negligible sound refraction effects for rays launched to the HARPs between 600 m depth and the seafloor [$< 2\ ms^{-1}$ change in sound speed according to Figure 3.3 (b)]. The source location candidates, $\mathbf{g}_{i,j,k}$, were distributed horizontally $\pm 5\ km$ and vertically from 300 to 1500 m depth with respect to the geo-referenced HARP C hydrophone to cover all potentially detectable Cuvier's beaked whale locations. For computational considerations, the horizontal and vertical resolution was initially 100 m to provide an overall sense of the beaked whale trajectories. Based on the initial results, the horizontal and vertical limits on the source location candidates were decreased, and the vertical and horizontal resolution was increased to 10 m (smaller than two times the length of a Cuvier's beaked whale).

To account for orders of magnitudes discrepancy between the small and large-aperture TDOAs, two likelihood surfaces, one for the small-aperture arrays, L_{sml}, and one for the large-aperture arrays, L_{lrg}, were defined. For each location candidate, $\mathbf{g}_{i,j,k}$, within the defined model space, the value of L_{sml} and L_{lrg} is computed respectively by

$$\begin{aligned} L_{sml}(\mathbf{g}_{i,j,k}) =& (2\pi\sigma_{sml}^2)^{-N/2} \\ & \times \exp\left(\frac{-1}{2\sigma_{sml}^2}\sum_{n=1}^{N}|TDOA_{smlmeas_n}[\mathbf{s_{Zc}}] - TDOA_{smlpred_n}[\mathbf{g}_{i,j,k}]|^2\right), \end{aligned} \tag{3.3}$$

$$\begin{aligned} L_{lrg}(\mathbf{g}_{i,j,k}) =& (2\pi\sigma_{lrg}^2)^{-M/2} \\ & \times \exp\left(\frac{-1}{2\sigma_{lrg}^2}\sum_{m=1}^{M}|TDOA_{lrgmeas_m}[\mathbf{s_{Zc}}] - TDOA_{lrgpred_m}[\mathbf{g}_{i,j,k}]|^2\right), \end{aligned} \tag{3.4}$$

where M represent the number of the measured large-aperture TDOAs with a maximum value of 10 for a click received on all five HARPs, and N equals the number of the measured small-aperture TDOA and is either 6 or 12 for a click received on one or two

small-aperture arrays, respectively.

The standard deviations σ_{sml} and σ_{lrg} scale L_{sml} and L_{lrg} while accounting for the aperture-dependent uncertainties in hydrophone locations and cross-correlation derived TDOA measurements

$$\sigma_{sml} = \sqrt{\sigma_{H_{sml}}^2 + \sigma_{xcorr_{sml}}^2}\,, \tag{3.5}$$

$$\sigma_{lrg} = \sqrt{\sigma_{H_{lrg}}^2 + \sigma_{xcorr_{lrg}}^2}\,, \tag{3.6}$$

with $\sigma_{H_{sml}} = 0.1 \times 10^{-3} s$ and $\sigma_{xcorr_{sml}} = 0.05 \times 10^{-3} s$ for the small-aperture array and $\sigma_{H_{lrg}} = 5 \times 10^{-3} s$ and $\sigma_{xcorr_{lrg}} = 0.3 \times 10^{-3} s$ for the large aperture array.

The source location, $\mathbf{s_{Zc}}$, is found by maximizing the combined likelihood surface, L. For each location candidate, $\mathbf{g}_{i,j,k}$, the value of L is computed by

$$L(\mathbf{g}_{i,j,k}) = L_{sml}(\mathbf{g}_{i,j,k}) L_{lrg}(\mathbf{g}_{i,j,k})\,. \tag{3.7}$$

Error estimates for a computed source location, $\mathbf{s_{Zc}}$, can be obtained from the 95% confidence intervals of the combined likelihood surface, L, for each of the three spatial dimension (Nosal and Frazer, 2007). For example, to estimate the error of x_{Zc}, the y and z values are kept fixed at the values of the estimated source location, y_{Zc} and z_{Zc}, to yield a conditional likelihood function (CLF), $L(x|y = y_{Zc}, z = z_{Zc})$. To identify the 95% confidence interval, a discrete cumulative CLF, $C(x)$, is computed:

$$C(x) = \sum_{x_i < x} L(x_i|y = y_{Zc}, z = z_{Zc}) \tag{3.8}$$

$C(x)$ is normalized by its maximum value so that its values range between 0 and 1. The

lower and upper limits of the 95% confidence interval of x_{Zc} are found by the x values that satisfy best $C(x_{2.5\%}) = 0.025$ and $C(x_{97.5\%}) = 0.975$, respectively, for the grid resolution of 10 m (Nosal and Frazer, 2007). For y_{Zc} and z_{Zc}, the 95% confidence intervals are obtained in the same fashion.

The 95% confidence intervals depend non-linearly on the source locations with respect to the HARP array and the number of HARPs that received the clicks. For horizontal locations inside the array and elevations of up to 300 m above the array, the 95% confidence intervals typically vary between $20-50$ m horizontally and between $30-80$ m vertically. For locations outside the array, but within 2 km horizontal and 800 m vertical radius, the horizontal and vertical location errors typically range between $40-70$ m and $60-140$ m, respectively.

3.3.4 Source time series and source levels

To account adequately for differences in the attenuation coefficient across a click's frequency bandwidth (> 5 dB/km between 30 and 50 kHz in Figure 3.4), source levels were estimated from source pressure time series in contrast to computing an apparent source level from the received pressure time series with an averaged, fixed attenuation coefficient [e.g. (Zimmer et al., 2005); (Shaffer et al., 2013)].

The source pressure time series of a click at a reference distance of 1 m, $s(t)$, is obtained by propagating the calibrated received pressure time series from the hydrophone along the computed slant range, r, in meters, back to the beaked whale, using a spherical propagation model and the frequency-dependent attenuation coefficient, $\alpha(f)$ in dB/km, with $\omega = 2\pi f$,

$$s(t) = \frac{r/1m}{2\pi} \int_{-\infty}^{+\infty} X(\omega)G(\omega)H(\omega)\mathrm{e}^{k\alpha(\omega)r}\mathrm{e}^{i\omega t}\,\mathrm{d}\omega\,. \tag{3.9}$$

In equation 3.9, $X(\omega)$ is the Fourier transform of the received acoustic pressure time series $x(t)$,

$$X(\omega) = \int_{-\infty}^{+\infty} x(t) \mathrm{e}^{-i\omega t}\, \mathrm{d}t \ . \tag{3.10}$$

The inverse Fourier and Fourier transforms of equation 3.9 and 3.10 were computationally implemented using a fast Fourier transform (FFT) algorithm.

$G(\omega)$ represents the inverse of the hydrophone-specific transfer function obtained from calibrations that were performed at the Scripps Whale Acoustics Laboratory and at the U.S. Navy's Transducer Evaluation Center facility in San Diego, California. $H(\omega)$ is a digital band-pass filter of order 64, which selects the frequency bands of $X(\omega)$ that are greater than 15 kHz and above the noise floor to retain only signal components introduced by beaked whales. The noise floor between 15 and 100 kHz is computed before each click and determines the number of the stop and pass bands with their corresponding cutoff frequencies for each received click individually. Power spectral density (PSD) levels of the noise floor were below 52 $dB\ re\ 1\ \mu Pa^2/Hz$ for all HARPs.

The constant k equals $[2*10^4*\log(e)]^{-1}$ and is required in equation 3.9 to convert the attenuation coefficient $\alpha(\omega)$ from dB/km to $Neper/m$ while the angular frequency dependence of $\alpha(\omega)$ maps to $\alpha(f)$ simply by $\omega = 2\pi f$. $\alpha(f)$ was computed (Ainslie and McColm, 1998) for the depth $(1000\,m)$ near which most of the Cuvier's beaked whale clicks were localized using a temperature of $4.1^\circ\,C$ and a salinity of 34.47 psu (practical salinity units) as measured by the two CTD casts. A pH of 7.3 was used, based on pH measurements up to 1100 m depth about 27 km west and east of the hydrophone array in 2013 [CLIVAR & Hydrographic Data Office; http://cchdo.ucsd.edu/cruise/318M20130321 (last viewed 25th June 2015)]. Variations of the attenuation coefficient due to changes in salinity, temperature and pH in the depth layer in which more than 95% of all

beaked whales were localized $(800-1200\ m)$ are negligible below 50 kHz and less than $\pm 1\ dB/km$ around 70 kHz (Figure 3.4).

Estimated directly from the computed source pressure time series, $s(t)$, of equation 3.9 were: (1) the peak to peak source level, SL_{pp}, (2) the total energy flux based on the 97% energy criteria, E_{97}, and in addition (3) the rms source level based on the 97% energy criteria, SL_{rms97}, to be consistent with the metrics used in previous literature for Cuvier's beaked whales and similar species [(Zimmer et al., 2005); (Shaffer et al., 2013)]. For calculating E_{97}, an average acoustic impedance $(1,531,500\ Rayl)$ was estimated from the CTD data for the water layer between 600 and 1200 m depth (Millero et al., 1980).

For the received and computed source pressure time series, calibrated energy spectral densities (ESD) in $dB\ re\ 1\ \mu Pa^2 s/Hz$ were computed, to avoid issues raised for PSD levels of transient sounds (Madsen, 2005). Note that the ESD levels differ from the PSD levels by $10\log(T_s)$, where T_s is the signal length.

3.3.5 Click directionality

To investigate the directionality of Cuvier's beaked whale clicks, each SL_{pp} of a click can be associated with an angle that is measured between the acoustic axis of the whales' click sound beam, and the vector connecting the whale with the HARP from which the SL_{pp} was estimated. This angle will be referred to as the off-axis angle, γ, and ranges from 0° (looking forward along the acoustic axis) over 90° (perpendicular to the acoustic axis) to 180° (looking backward along the acoustic axis). Assuming that the acoustic axis of the whale's click beam was parallel to the whale's velocity vector during clicking, off-axis angles of clicks received at the HARPs with 100 kHz bandwidth

(HARPs N, E and S) were obtained by

$$\gamma = \sqrt{(\alpha')^2 + (\phi')^2}\,, \tag{3.11}$$

with

$$\alpha' = \tan^{-1}\left(\frac{b'_y}{b'_x}\right) \tag{3.12}$$

and

$$\phi' = \tan^{-1}\left(\frac{b'_z}{\sqrt{(b'_y)^2 + (b'_x)^2}}\right) \tag{3.13}$$

b'_x, b'_y and b'_z are the components of the whale frame direction vector, $\mathbf{b}'$, and were computed according to equation 9 and 16 in (Nosal and Frazer, 2007). Due to the insensitivity of γ to the whale's rotation around its acoustic axis, the matrix accounting for the whale's roll movements in equation 9 in (Nosal and Frazer, 2007) was omitted. The required time-varying velocity vector, $\mathbf{v}(t) = (v_x(t), v_y(t), v_z(t))$, was smoothed by computing the first derivative of the $x(t)$, $y(t)$ and $z(t)$ component of the Cuvier's beaked whale track $\mathbf{s_{Zc}}(t)$ over a sliding time window of 20 s using linear regression.

For comparison, the broadband beam pattern of a flat circular piston model with a diameter of 0.5 m was implemented according to equation 4 - 6 in (Zimmer et al., 2005). For the Gaussian frequency weighting function in equation 9 in (Zimmer et al., 2005), a center frequency of 42.1 kHz and a bandwidth of 7.9 kHz were used. The DI of the piston model was computed according to equation 7 in (Zimmer et al., 2005).

3.4 Results

Using the method described above, Cuvier's beaked whales were tracked within approximately 2.5 *km* with respect to the center of the hydrophone array at HARP C. A total of 11 tracks of Cuvier's beaked whales are shown in Figure 3.5. These tracks include two encounters of single individuals [Figure 3.5 (a) and (b)], three encounters of two individuals [Figure 3.5 (c) - (e)] and one encounter of three individuals [Figure 3.5 (f)]. The individual tracks will be referred to as a combination of the subplot number and, if multiple individuals are present, the track color. For example, the green track in subplot (c) of Figure 3.5 will be referred to as 5(c) green.

Based on multiple-individual encounters [Figure 3.5 (c) - (f)] individuals within the tracked groups are less than 1.5 *km* apart from each other during the encounter and are traveling, with respect to each other, in the same general direction with the exception of one Cuvier's beaked whale, which reversed its initial westward travel direction [5(c) green]. Another example of a beaked whale reversing its direction [5(b) from south to north between 22:19 - 22:24 GMT] occurred following its initial dive descent.

Buzzes were detected at the locations of the orange asterisks in Figure 3.5 (c) as two Cuvier's beaked whales approach each other (blue and green track) at a depth of 1240 *m* (elevation of 60 *m* above seafloor) and in Figure 3.5 (e) (blue track) at depth of 1090 *m* (elevation of 140 *m* above seafloor). The maximum peak to peak source level of the individual buzz clicks from each of the two buzz sounds were estimated from HARP N is 177 *dB re* 1 μPa @ 1 *m* and 179 *dB re* 1 μPa @ 1 *m*, respectively. The minimum ICI of the buzzes were 5.6 *ms* [Figure 3.5 (c)] and 7.3 *ms* [Figure 3.5 (e)].

The maximum duration and length of the tracks were 33 *min* [5(e) blue] and 2.9 *km* [5(d) blue], respectively. The average horizontal movement speed of each of the 11 tracks varies between 1 and 3 ms^{-1}. Foraging elevation varies greatly during and

between the 11 individual tracks from seafloor depth to 400 *m* above the local seafloor.

3.4.1 Dive behavior and varying inter-click-interval

Dive and clicking behavior results are exemplified by the track of the Cuvier's beaked whale 5(b). The depth profile and the corresponding ICI as a function of time for this track are shown in Figures 3.6 (a) and (b), respectively. Over a period of 4 *min*, the single individual descends from about 500 to 1000 *m* depth, halting the descent at about 300 *m* above the local seafloor. During this period, the whale alternates between two ICI regimes as it reduces the time interval between clicks from about 0.6 to 0.3 *s* for one regime and from 0.9 to 0.55 *s* for the other regime [Figure 3.6 (b)]. At any given time, the two ICI rates are not related by a simple multiple, suggesting that a single interval with occasional skipping of clicks does not explain the timing.

Instead, it appears that the whale is purposely altering the ICI during its descent, both by gradually increasing the overall rate of clicking, and by alternating between a faster and slower clicking regime.

After 22:24 GMT, the Cuvier's beaked whale gradually ascends and descends three times (minimum of 875 *m* and maximum of 1050 *m*) as it moves north and westwards over a gently sloping bottom [Figures 3.5 (b) and Figure 3.6 (a)]. During this, presumably, foraging part of the dive, the ICI of 5(b) oscillates around a median of 497 *ms*, but has short-term patterns of ICI variation, as well as several gaps in clicking of several second duration.

The tracks of 5(d) green and 5(e) blue also contain a descent accompanied by two similar alternating and decreasing ICI regimes, followed by oscillations around a median ICI of approximately 500 *ms* during the foraging part of the dive. The other 9 tracks show similar ICI oscillations, but contain neither a descent part nor two alternating and decreasing ICI regimes, presumably because these portions of the dive were beyond

the range of the array where tracking was possible.

3.4.2 Click directionality

The beam pattern of the echolocation clicks, coupled with changes in direction of the animals, resulted in large changes in received signal levels and subsequent non-beam angle corrected (NBAC) source level estimates, as illustrated for track 5(b) in Figure 3.7. The click peak-to-peak NBAC source levels of 5(b) varied between 160 and 224 $dB\ re\ 1\ \mu Pa\ @\ 1\ m$ as estimated from HARPs N, E and S [Figure 3.7 (a) - (c)]. The remainder of this section relates the variations of the click peak-to-peak NBAC source levels of 5(b) to its three-dimensional track and concludes with a quantitative description of its directionality.

During the descent of 5(b) towards the ocean floor approximately 1.5 km south of the center of the HARP array, it is apparent that its echolocation beam sweeps twice over the HARP array within the first few minutes causing the SL_{pp} to rise twice up to about 215 $dB\ re\ 1\ \mu Pa\ @\ 1\ m$ [Figure 3.7 (c)] and to drop below 195 $dB\ re\ 1\ \mu Pa\ @\ 1\ m$ in between [Figure 3.7 (a) - (c)]. As 5(b) transitioned from the descent to the foraging part of the dive at 22:23 GMT, no clicks were detected on any of the five HARPs for 45 s. However, when 5(b) started the foraging part of its dive northwards towards the HARP array shortly after 22:24 GMT, the SL_{pp} increased rapidly to 224 $dB\ re\ 1\ \mu Pa\ @\ 1\ m$ on HARP E [Figure 3.7 (b)], which is a source level 10 dB higher than previously reported for Cuvier's beaked whales (Zimmer et al., 2005).

As 5(b) approached the HARP array horizontally by traveling northwards [Figure 3.5 (b)], but simultaneously ascended by approximately 200 m [Figure 3.6 (a)], the SL_{pp} decreases on HARPs N, E and S by more than 20 dB (Figure 3.7). This trend is reversed rapidly on HARPs N and E as 5(b) turned sharply westward and started to descend towards the HARPs around 22:27 GMT. During this maneuver, it emitted a click towards

HARP N with a SL_{pp} of 222 $dB\ re\ 1\ \mu Pa\ @\ 1\ m$ as its beam moved counter-clockwise through the array from HARP E over N to S.

During the final portion of the track, 5(b) finished its turn and headed westward, the SL_{pp} on HARP S increased dramatically by more than 20 dB until 22:29 GMT while the SL_{pp} decreased simultaneously on HARPs N and E. After 22:29 GMT, 5(b) started to head northwest and to ascend, which coincided with a dramatic decrease of SL_{pp} to 160 $dB\ re\ 1\ \mu Pa\ @\ 1\ m$ on HARP S compared to a moderate decrease of SL_{pp} on HARPs N and E to 172 $dB\ re\ 1\ \mu Pa\ @\ 1\ m$ despite the close horizontal proximity of 5(b) to HARP S [Figure 3.5 (b), Figure 3.6 (a) and Figure 3.7]. As 5(b) descended towards the seafloor around 22:33 GMT, the SL_{pp} on HARP S increased strongly to SL_{pp} of 180 $dB\ re\ 1\ \mu Pa\ @\ 1\ m$, which is similar to HARPs N and E.

To quantitatively characterize the directionality of the echolocating Cuvier's beaked whale 5(b), the SL_{pp} estimates from HARPs N, E and S (total of 2055 estimates), as shown in Figure 3.7 (a) - (c), were plotted against their off-axis angles as blue, green and red dots, respectively (Figure 3.8). The ten clicks with the highest SL_{pp} between 210 and 224 $dB\ re\ 1\ \mu Pa\ @\ 1\ m$ define the peak of the $SL_{pp}(\gamma)$ distribution at off-axis angles in the vicinity of 30°, which reveals the actual acoustic axis of the click's sound beam. Hence, such clicks will be referred to as either on-axis or near on-axis clicks depending on their SL_{pp} and their near-alignment to estimated axis of the whales' sound beam. For off-axis angles smaller or greater than 30°, the $SL_{pp}(\gamma)$ distribution decreases dramatically by several tenths of dB despite its high variations ($> 10\ dB$). A radial broadband piston beam pattern (black line in Figure 3.8) was fitted to the $SL_{pp}(\gamma)$ distribution with a piston diameter of 0.5 m and a corresponding DI of 30 dB, which is within the DI range previously reported for Cuvier's beaked whales (Zimmer et al., 2005).

3.4.3 Energy spectral density and high-frequency components

The on-axis click ($\gamma = 32^{\circ}$) highlighted by a leftward arrow in Figure 3.7 (a) and Figure 3.8 has a SL_{pp} of 222 $dB\ re\ 1\ \mu Pa$ @ 1 m, a SL_{rms97} of 205 $dB\ re\ 1\ \mu Pa$ @ 1 m and a total energy flux (E_{97}) of 172 $dB\ re\ 1\ \mu Pa^2\ s$ @ 1 m. Its spectral and temporal properties are shown in Figure 3.9. The estimated energy spectral density (ESD) of the click at the reference distance of 1 m from 5(b) [blue line Figure 3.9 (a)] shows that the majority of click energy is concentrated between 40 and 60 kHz with a side lobe at 23.3 kHz that is 23 dB lower than the maximum of the main lobe at 47.8 kHz. This spectral shape is consistent with what has been previously reported (Zimmer et al., 2005). However, there are two additional high-frequency lobes at 72.2 and 91.1 kHz present in the source ESD estimated at 1 m that are, respectively, 6 and 9 dB lower than the maximum of the main lobe. Note, that for the ESD of the click received at HARP N at 1 km distance from 5(b), the two high-frequency lobes are 11 and 20 dB lower than the maximum of the main lobe at 58 $dB\ re\ 1\ \mu Pa^2\ s/Hz$ @ 1 km [solid green line in Figure 3.9 (a)], but well above the noise floor [green dotted line in Figure 3.9 (a)] by more than 10 dB. In addition, the 91.1 kHz lobe is 14 dB higher than the 23.3 kHz lobe in the source ESD at 1 m distance in contrast to the ESD received at 1 km distance, where the 91.1 kHz lobe is 4 dB lower than the 23.3 kHz lobe. This is due to the high absorption of sound in seawater at high frequencies in conjunction with the strong frequency dependence of the sound absorption over the bandwidth of the Cuvier's beaked whale click (3 dB/km at 20 kHz in contrast to 22 dB/km at 90 kHz as illustrated in Figure 3.4).

The high frequency components of the click are present between 0.085 and 0.295 ms while the main lobe is a frequency-modulated upsweep that lasts until 0.4 ms as shown in the source pressure time series at 1 m and in the spectrogram [Figure 3.9 (b) and (c)]. Near on-axis clicks with frequency components above 60 kHz have also been

observed for all of the other 10 Cuvier's beaked whale tracks at all HARPs sampling at 200 kHz (N, E and S). However, the 90 kHz lobe is not present in the received ESD of these near on-axis clicks if the distance between the Cuvier's beaked whale and the recorder is greater than 1 km, such as for the near on-axis click emitted by 5(b) at 1.4 km distance from HARP N with an SL_{pp} of 224 $dB\ re\ 1\ \mu Pa$ @ 1 m.

3.5 Discussion

Uncertainties in the HARP locations, small-aperture array orientations, cross-correlation based TDOAs and time-synchronizations reduce the accuracy of the maximum likelihood estimator's click localization estimates, so only movement features greater than $10-20\ m$ can be resolved within $1-3\ km$ distance from the array. To resolve movements on finer scales, for example, to investigate foraging helical movements (Johnson et al., 2004), advanced tracking or smoothing filters can be applied to echolocation tracks from locations.

Although the localization method used here allows the use of an acoustic propagation model such as BELLHOP (Porter, 2005) instead of a spherical propagation model with a constant sound speed, there is no significant advantage in using a ray-trace model such as BELLHOP for deep-diving Cuviers' beaked whales below 500 m due to the negligible changes in sound speed at these depths. The difference in travel time of a ray obtained from a spherical propagation model with a constant sound speed of 1484 ms^{-1} versus BELLHOP with the depth-dependent sound speed profile is less than 1 ms for a 45 kHz source at 500 m depth at 2 km distance from a seafloor HARP. Given the uncertainties in the HARP location estimates of 4 m (equivalent to a travel time of approximately 3 ms using a sound speed of 1484 ms^{-1}) and the limited accuracy of the eigenray-tracing capabilities of BELLHOP, we decided to use the spherical propagation model with a constant sound speed of 1484 ms^{-1}. Even for the surface locations of the

ship tracks that were used to calibrate the small-aperture array orientation, the difference in arrival angle of a straight path and the eigenray connecting the surface ship and a four-channel HARP is less than 0.07° at the four-channel HARP for ranges smaller than the water depth. This slope difference maps into a horizontal displacement of the surface ship of less than 25 m, which is less than the length of the ship (R/V Sproul) generating the sound. Furthermore, the high-resolution bathymetry data (obtained from the multibeam sonar survey during the R/V Revelle cruise CNTL05RR) needed to be adjusted to match the depths of the five HARPs to less than a few tens of meters.

Although information from tagged Cuvier's beaked whales suggests 30 buzzes per dive (Tyack et al., 2006), only two buzz sound events were detected for the 11 Cuvier's beaked whale tracks. This low number may result from a lower detectability for buzzes due to lower source levels compared to clicks and also from different animal behavioral states that potentially could lead to fewer buzz sounds.

The use of alternating ICI regimes during the descent phase of the dive [Figure 3.6 (b)] warrants further examination. At 22:21 GMT in Figure 3.6, the animal is located at 600 m above the seafloor (740 m depth with 1340 m seafloor) and is using about 0.8 s for the long ICI regime; this delay is needed to wait for the seafloor echo to return before emitting another click. Likewise, at the end of the descent phase of the dive (22:23) GMT, the animal is about 340 m above the seafloor (1000 m depth with 1340 m seafloor) and using a 0.59 s long ICI, somewhat greater than what is needed for the seafloor echo to return. The short ICI regime, on the other hand, is consistently more rapid than the delay needed for the seafloor echo. This suggests that the animal may switch between these two regimes to both avoid ambiguity about the distance to the seafloor (long ICI regime) as well as to obtain closer echo information more rapidly (short ICI regime).

Despite frequent variations of over 40 dB, peak-to-peak source levels above 210 $dB\ re\ 1\ \mu Pa\ @\ 1\ m$ are sparse for any given Cuvier's beaked whale track and for

any of the five HARPs. This suggests that the acoustic axis of the Cuvier's beaked whale is rarely aligned with any of the seafloor HARPs. Uncertainty in the source level estimates are mainly driven by uncertainties in the localization with an upper limit of 3 dB and therefore, cannot explain the occasional presence of source levels up to 224 dB re 1 μPa @ 1 m. Although equation 3.9 recovers the magnitude of the high-frequency components of a click, these components do not contribute significantly to the peak-to-peak source level since the majority of the signal energy is contained in the frequency modulated upsweep between 40 and 60 kHz. Furthermore, the attenuation in sound intensity takes into account the sound absorption in seawater while ignoring scattering from inhomogeneities in the water such as prey items, since their distribution and properties are unknown. The increasing dependence of sound absorption on depth, temperature and conductivity with increasing frequency causes uncertainties of less than 0.5 to 1 dB/km for frequencies between 70 and 90 kHz in the energy spectral density estimate of a click (Figure 3.4), but because of the relatively short ranges (< 2.5 km), these uncertainties are not significant. Despite small errors at higher frequencies, the remaining variations in the energy spectral densities of clicks are likely caused by natural variations in the Cuvier's beaked whale's click sound production and by the orientation of the acoustic axis of the Cuvier's beaked whale with respect to the hydrophone.

The large variations in the $SL_{pp}(\gamma)$ distribution are mainly driven by the uncertainties in the off-axis angle estimations rather than by the peak-to peak source level estimations (errors ≤ 3 dB as discussed above) if the natural variations in click directivity and peak-to-peak source level are assumed to be negligible. Uncertainties in the off-axis angles result from errors in estimating the whale's velocity vector and from its misalignment with the whales' acoustic axis during clicking due to head and yaw movements. The velocity vector is estimated as the first derivative of the linearly smoothed track 5(b) and hence, would benefit from applying more advanced tracking or smoothing filters

to the track. This would not only help to reduce some of the variations in the $SL_{pp}(\gamma)$ distribution, but might also help to reduce the number of outliers (i.e. located between 90° and 180° at around 200 $dB\ re\ 1\ \mu Pa$ @ 1 m in Figure 3.8). The misalignment between the whale's acoustic axis and velocity vector could potentially also explain the presence of the $SL_{pp}(\gamma)$ distribution's peak at approximately 30°. In a previous, tag-based study of Cuvier's beaked whales, the $SL_{pp}(\gamma)$ distribution peaked at an off-axis angle between 18° and 35° (Zimmer et al., 2005). In addition, the sound beam of echolocating Cuvier's beaked whales may be expected to not be aligned with the rostral axis of the marine mammal due to significant bilateral asymmetry (Cranford et al., 2008). Hence, the 30° offset of the $SL_{pp}(\gamma)$ distribution's peak could be, at least partly, caused by this phenomena, which remains subject to further investigation.

The high-frequency components above 60 kHz in Figure 3.9 are unlikely to be harmonic distortions caused by non-linear effects of the analog recording chain between hydrophone and input of the analog-digital converter. Despite the high source levels of these clicks, their received levels are approximately 10 dB below the clipping levels of the HARPs and at these levels non-linear effects can be considered negligible.

3.6 Conclusions

By embedding volumetric small-aperture ($\approx 1\ m$ element spacing) arrays into a large-aperture ($\approx 1\ km$ element spacing) seafloor array, highly directional and deep-diving sound sources such as echolocating beaked whales can be tracked in all three spatial dimensions without relying on boundary reflections or depth information from suction-cup tags. The 11 Cuvier's beaked whale tracks presented here show movements of individuals as well as coordinated behavior within groups of up to three individuals over time periods from 10 to 33 min in an area of 20 km^2 around the center of the array. Beaked whale elevation above the seafloor varied during the foraging part of the dive

by more than one hundred meters and between individuals from several tens of meters to several hundreds of meters. During the tracked descents of the dives, the Cuvier's beaked whales reduced gradually their ICI while alternating between two ICI regimes, apparently as means for tracking both their height above the seafloor and closer features.

For the localized echolocation clicks of one individual, peak-to-peak source levels of up to 224 $dB\ re\ 1\ \mu Pa\ @\ 1\ m$ with a DI of 30 dB were estimated. The estimated source energy spectra at 1 m of the on-axis clicks show significant frequency components above the previously described FM upsweep. For buzz sounds, the maximum peak-to-peak source level was estimated to be 179 $dB\ re\ 1\ \mu Pa\ @\ 1\ m$. In addition, this passive acoustic tracking technique has the potential to collect large numbers of tracks over long periods to study three-dimensional movement patterns of deep-diving, echolocating odontectes without or with the presence of manmade noise.

3.7 Acknowledgments

Funding for this research was provided by the US Navy CNO-N45, the Naval Postgraduate School, Office of Naval Research, and the University of California ship fund program for young investigators. We thank Frank Stone, Ernie Young, Bob Gisiner, Curt Collins, John Joseph, Mike Weise and Bruce Applegate for support and assistance. We also thank Mike Buckingham and Bill Hodgkiss for helpful discussion as well as the Scripps Whale Acoustics Lab members, especially Marie Roch and Simone Baumann-Pickering.

Chapter 3, in full, has been accepted for publication of the material as it will appear in Gassmann, M., Wiggins, S. M., and Hildebrand, J. A. Three-dimensional tracking of Cuvier's beaked whales' echolocation sounds using nested hydrophone arrays. *The Journal of the Acoustical Society of America*, in press. The dissertation author was the primary investigator and author of this paper.

Table 3.1. Location and configuration of the High-frequency Acoustic Recording Packages (HARPs). Latitude, longitude and depth of redeployed HARPs E and S are given in parentheses.

HARP Site Name	**Number of hydrophones**	**Sampling frequency [kHz]**	**Latitude [North]**	**Longitude [West]**	**Hydrophone depth [m]**
C	1	200	32° 22.194’	118° 33.774’	1263
N	4	100	32° 22.414’	118° 33.781’	1256
E	1	200	32° 22.168’ (32° 22.188’)	118° 33.464’ (118° 33.535’)	1227 (1235)
S	1	200	32° 21.922’ (32° 21.906’)	118° 33.789’ (118° 33.831’)	1277 (1282)
W	4	100	32° 22.209’	118° 34.137’	1310

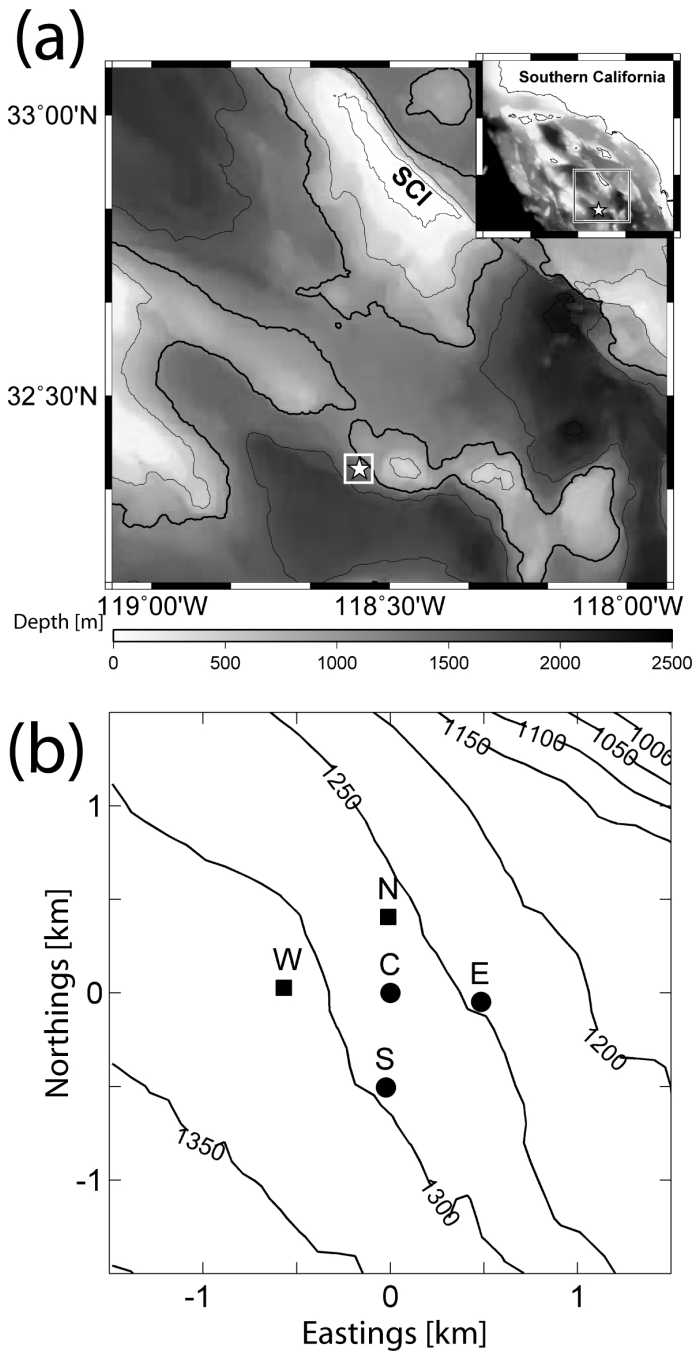

Figure 3.1. (a) Location of the acoustic tracking array (star in the square box) in the Southern California Bight south of San Clemente Island (SCI). Black bathymetry contour lines are shown every 500 *m*. (b) Map of the seafloor array with five HARPs (C, N, E, S, and W) geo-referenced to HARP C (32° 22.194' N 118° 33.774' W). Circles and squares represent HARPs with one hydrophone or with a small-aperture array, respectively. High-resolution bathymetry was obtained from a multibeam SONAR scan on the R/V Revelle cruise CNTL05RR. Depths of contours are in meters below sea surface.

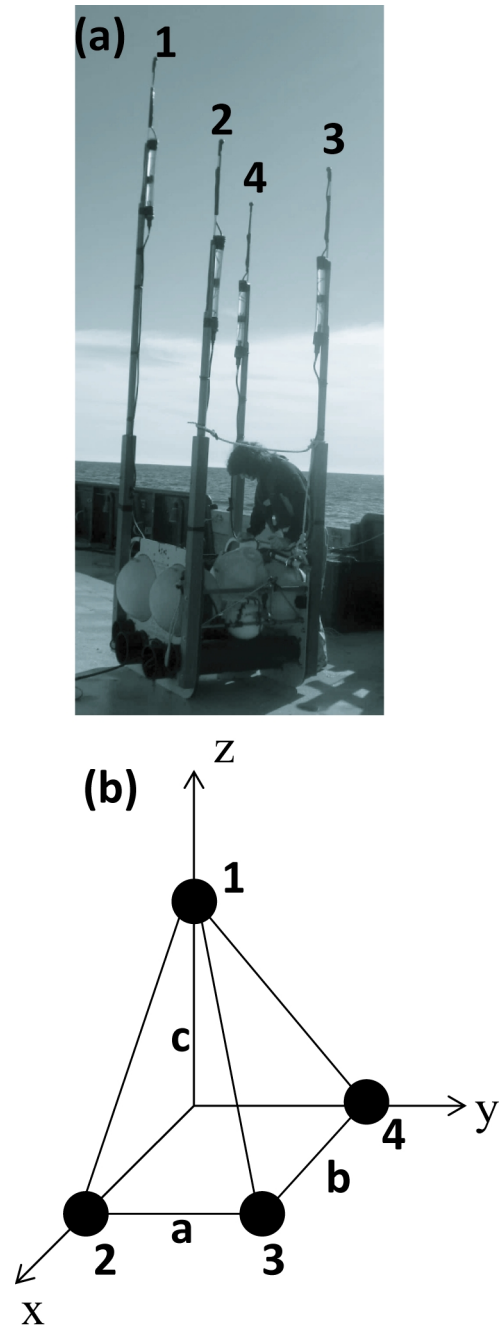

Figure 3.2. (a) Small-aperture array of four hydrophones at the top of each vertical mast as indicated by the numbers 1 through 4, located above a HARP seafloor package. (b) Schematic of the small-aperture array configuration with its spacing $a = 0.9\ m$, $b = 1.1\ m$ and $c = 0.9\ m$.

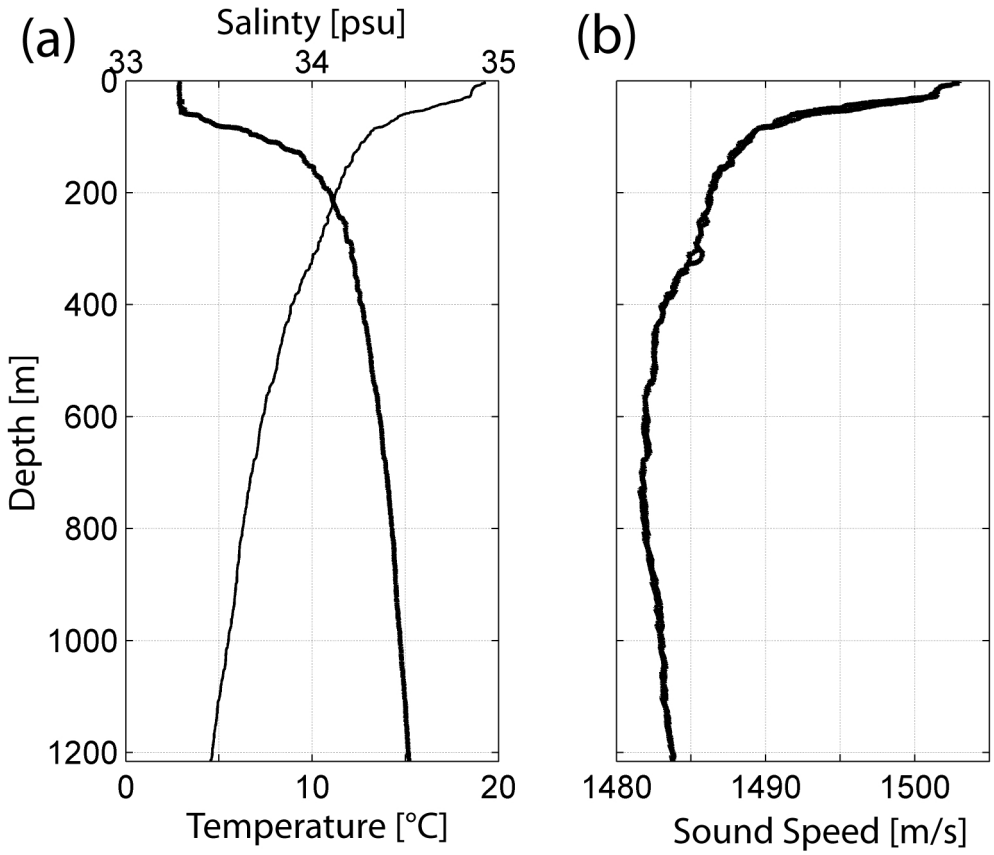

Figure 3.3. Salinity, temperature and sound speed profile. (a) Salinity (thick line with upper horizontal scale) and temperature (thin line with lower horizontal scale) profile from surface-to-near seafloor, down and upward CTD cast near HARP N. (b) Estimated sound speed profiles according to (Del Grosso, 1974) based on temperature and salinity profiles from (a).

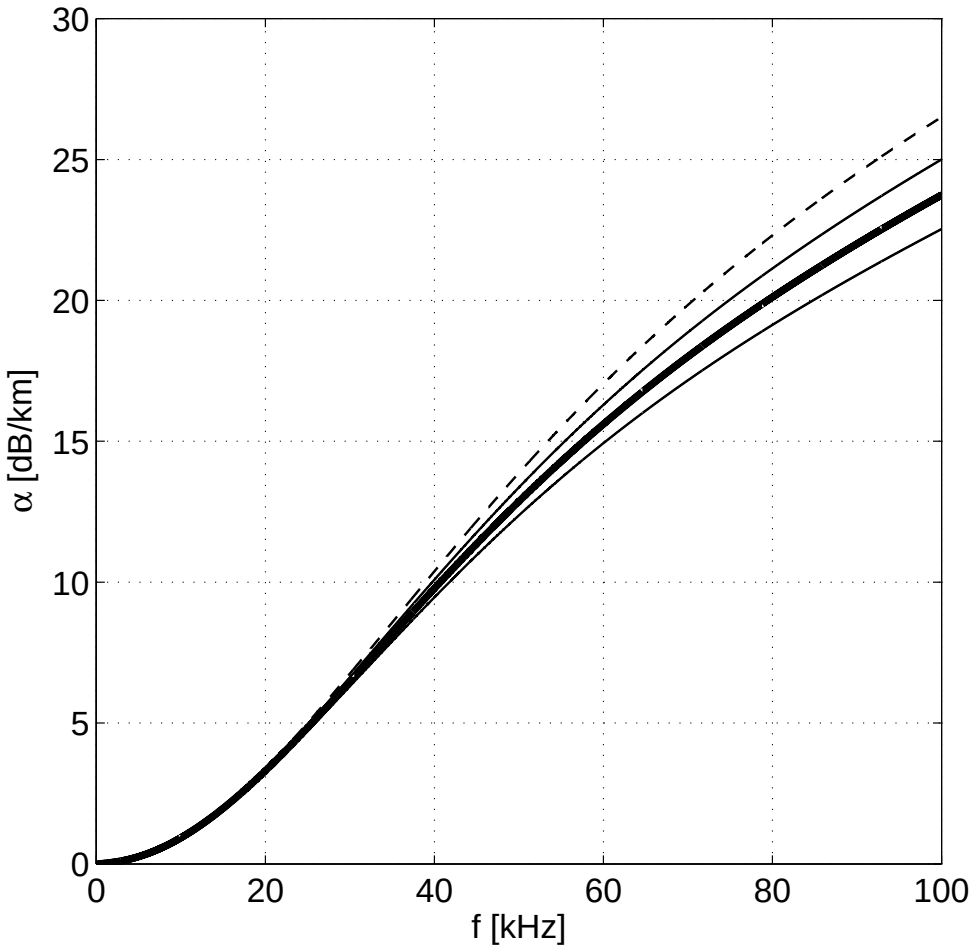

Figure 3.4. Sound absorption coefficient α as a function of frequency (Ainslie and McColm, 1998) at the HARP array based on the CTD data shown in Figure 3.3 (a) for a pH of 7.3. Thick line represents α at 1000 *m* and is used in equation 3.9. Depth, temperature and salinity dependence of α is illustrated by the lower solid, upper solid and dashed line for the CTD data at 1200 *m*, 800 *m* and 600 *m* depth, respectively.

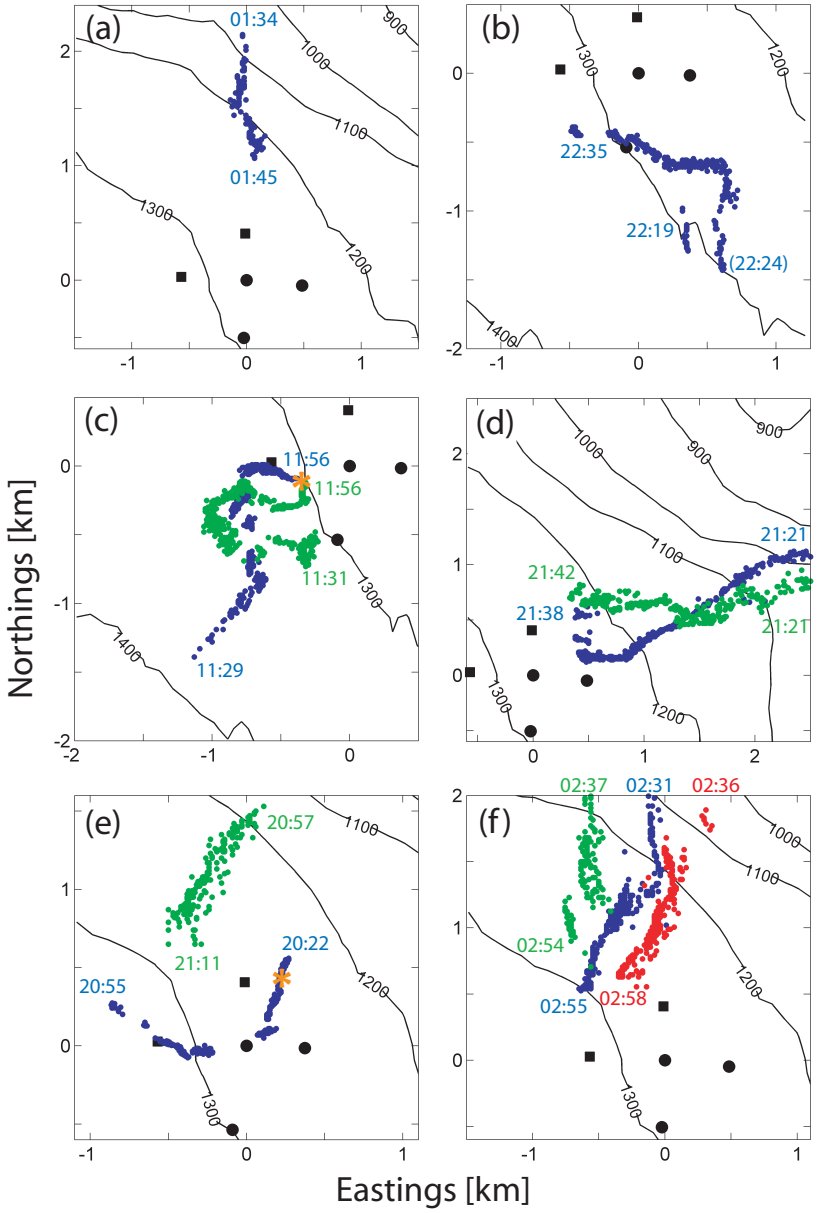

Figure 3.5. Six maps of 11 tracks of Cuvier's beaked whales (color dots) with respect to the HARP array (black squares and circles) showing two singles (a) and (b), three groups of two individuals (c) through (e), and one group of three individuals (f). Blue, green and red color of dots distinguishes between different individuals within a group. Locations of buzzes are indicated by orange asterisks in (c) and (e). Start and end times of each track are shown in GMT in hh:mm format for December 29, 2010 (a), February 7, 2011 (b), January 7, 2011 (c), December 19, 2010 (d), January 9, 2011 (e) and December 29, 2010 (f). Time in parentheses in (b) indicates transition between descending and foraging part of dive. Black contour lines represent water depth in meters. (b), (c) and (e) show HARP array with the locations of the redeployed HARPs E and S.

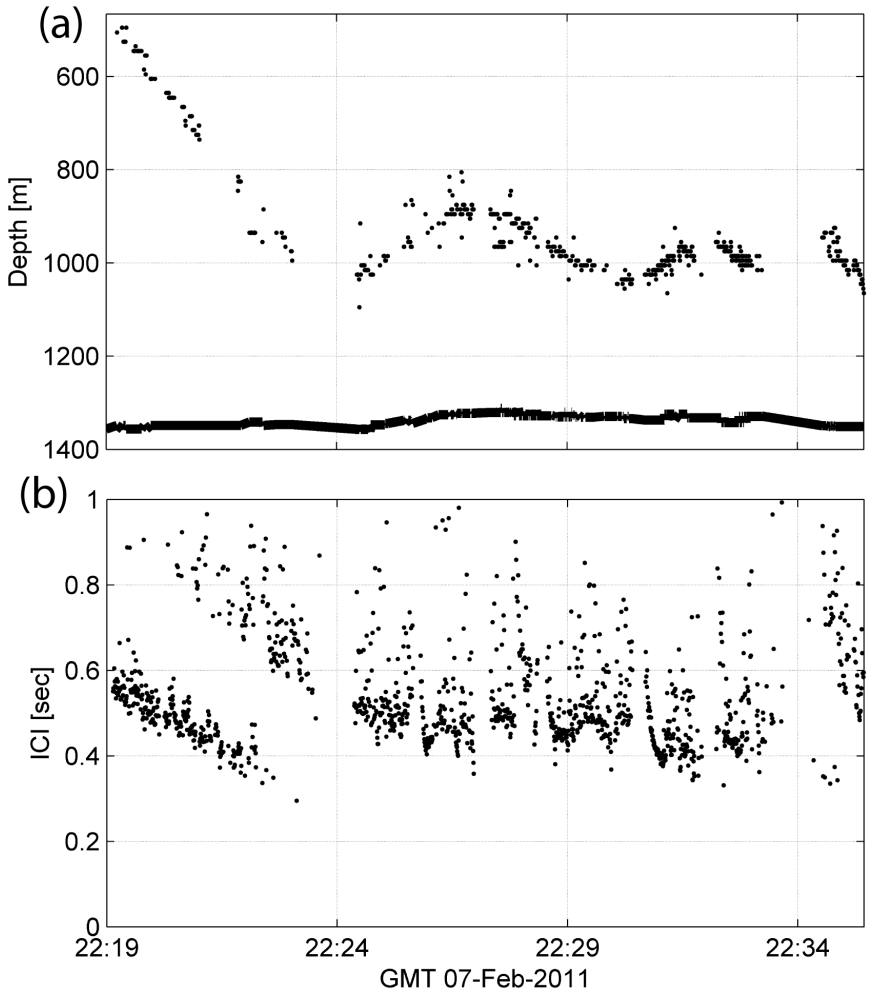

Figure 3.6. Depth profile of Cuvier's beaked whale track from Figure 3.5 (b) and corresponding inter-click interval (ICI) recorded on HARP N [panel (a) and (b) respectively]. Local seafloor is indicated by the thick black line in panel (a).

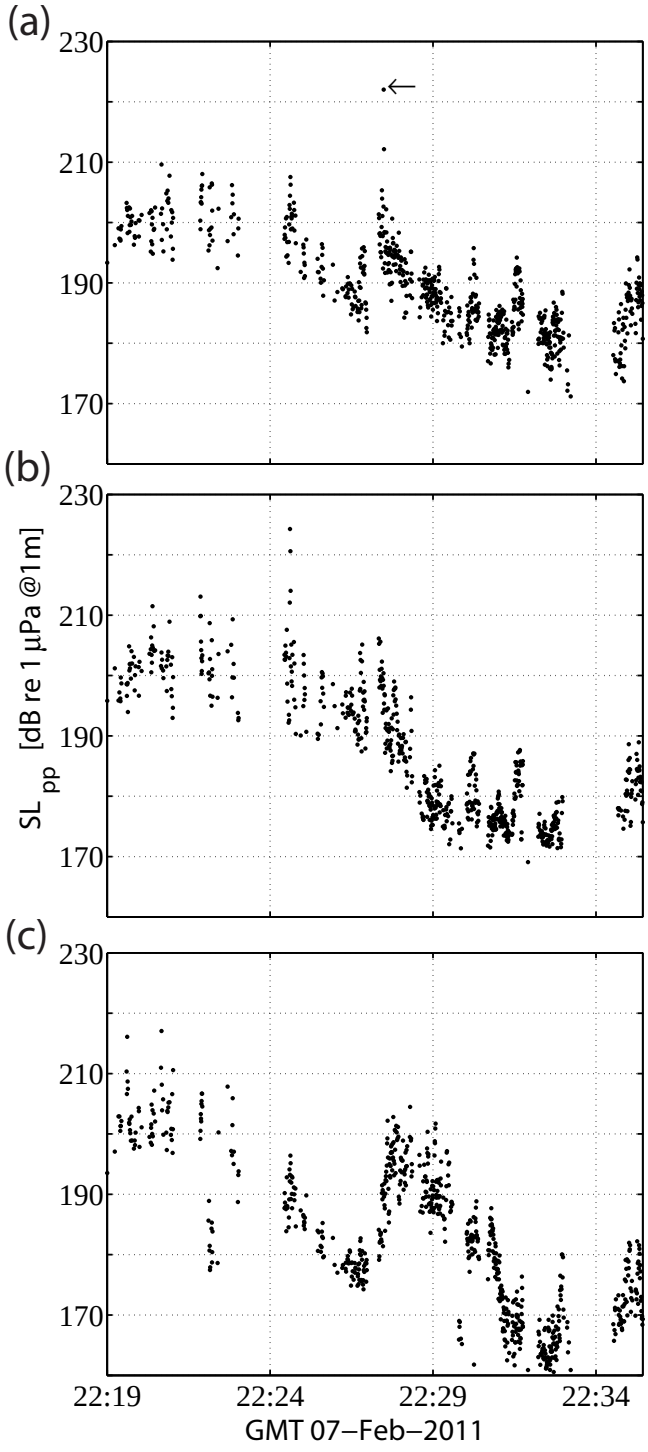

Figure 3.7. Peak to peak source level estimates (SL_{pp}) of clicks recorded on HARPs N (a), E (b) and S (c) for the track in Figure 3.5 (b) and Figure 3.6. Leftward arrow in (a) highlights the on-axis click discussed in section 3.4.3.

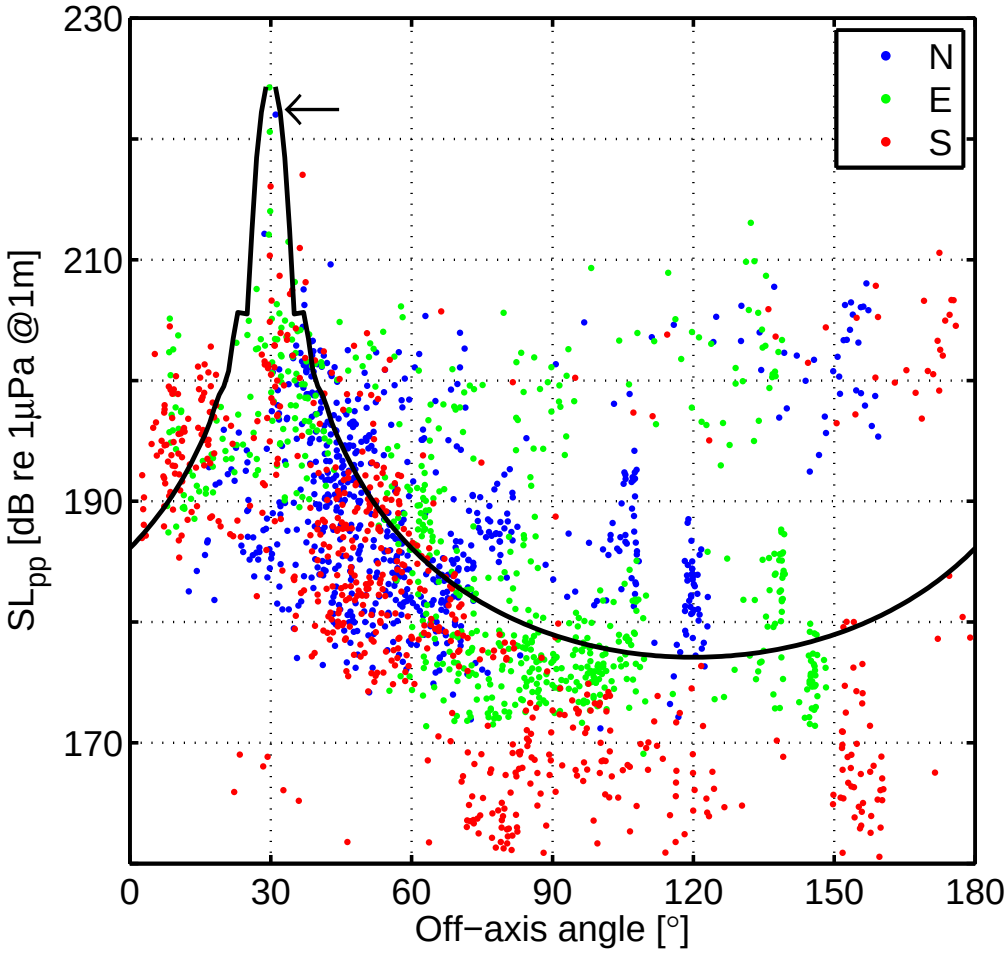

Figure 3.8. Peak to peak source level estimates (SL_{pp}) of 2055 clicks as a function of off-axis angle for the track in Figure 3.5 (b) and Figure 3.6. Clicks received by HARPs N, E and S are represented by the blue, green and red dots, respectively, and correspond to the clicks shown in Figure 3.7 (a) - (c). Black line represents a piston model with a diameter of 0.5 *m*. Leftward arrow highlights the on-axis click discussed in section 3.4.3.

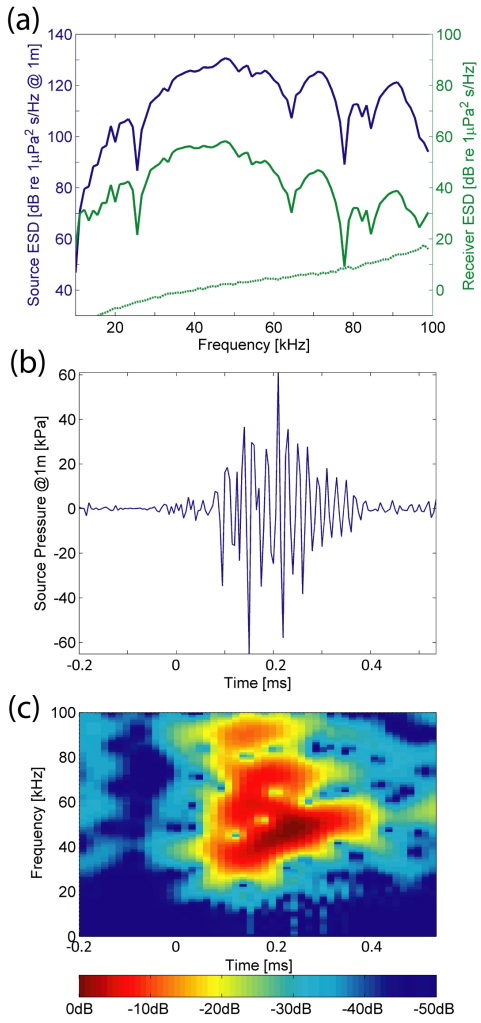

Figure 3.9. On-axis beaked whale click: (a) source (blue) and received (green) energy spectral density (ESD), along with equivalent instrument noise floor (dotted green), (b) source pressure time series, and (c) normalized source spectrogram. Source ESD and pressure time series at a reference distance of 1 m were estimated for a click received by HARP N at a slant range of 1 km [click highlighted by leftward arrow in Figure 3.7 (a) and Figure 3.8]. The source ESD is referenced to the left vertical axis, whereas the received ESD and noise floor share the right vertical axis in (a). Strongly attenuated ($> 10\ dB/km$) frequency components above 40 kHz in the received ESD are recovered in the source ESD according to equation 3.9. Note that the noise floor is at least 10 dB below the received ESD, except for the vicinity of 78 kHz. The click's total energy flux is 172 $dB\ re\ 1\ \mu Pa^2\ s$ @ 1 m and its peak to peak source level is 222 $dB\ re\ 1\ \mu Pa$ @ 1 m, estimated from the source pressure time series in (b). Source spectrogram in (c) was calculated with 32 sample FFTs with 90% overlap from the source pressure time series in (b) and normalized by its maximum.

Chapter 4

Tracking and measuring underwater radiated sound from ships with a small-aperture seafloor array

4.1 Abstract

To track and measure the underwater radiated sound of surface ships, a frequency domain beamformer (FDB) was implemented for a volumetric hydrophone array ($< 2\,m$ element spacing) that was coupled to an autonomous acoustic seafloor recorder. While the FDB yields estimates of magnetic bearings and vertical angles, ranges to the surface ships are triangulated by assuming straight ray paths. To illustrate the method, six ship tracks and their corresponding source spectra at the closest point of approach (CPA) are shown. The method is confirmed by comparing the acoustically derived ship track of the car carrier 'Solar Wing' with its track from the automatic identification system (AIS). The directionality of the underwater radiated sound of one ship was characterized with the waist and bow being respectively 3 and 8 dB quieter than the stern of the ship.

The method allows for tracking and measuring underwater radiated sound from ships of opportunity with a single-instrument deployment without requiring any AIS ship track information. In addition, the beampattern of the FDB provides a tool to investigate the bottom reflections of the ship sound and their contributions to the source

level estimation of ships near the seafloor.

4.2 Introduction

Commercial shipping is a significant contributor to low-frequency ambient noise in the ocean [e.g. (Wenz, 1962) and (Hildebrand, 2009)]. The underwater radiated sound of surface ships is dominantly, yet unintentionally caused by propeller cavitation (Ross, 1976) within a frequency range of $50 - 150\,Hz$ at which sound propagates long ranges due to little attenuation by absorption and scattering ($< 10^{-2}\,dB/km$).

To study the impact of low-frequency ship sound on marine organisms such as marine mammals, a description of the underwater radiated sound for a large number of individual ships under normal operation conditions is desirable in general, and also for particular areas such as marine mammal sanctuaries. For example, (McKenna et al., 2013) conducted measurements for a large number of ships of opportunity (SoO) in the Santa Barbara Channel near the ports of Los Angeles/Long Beach with a single, bottom-mounted hydrophone, while relying on data from the automatic identification system (AIS) for the tracks and speeds of the ships. However, AIS data is not available for all ships and is also not available in all areas of the world as most ships use very-high-frequency (VHF) based AIS systems that require a nearby VHF receiver, e.g. at an island. This limits the applicability of this technique geographically as well as the number of SoOs that can be measured.

In this chapter, a passive acoustic method that allows for tracking and measuring of any SoO with a single-instrument deployment, but without relying on AIS data, is described. The ship tracking method based on frequency domain beamforming (FDB) with a small-aperture volumetric seafloor array is presented in section 4.3. To illustrate the method, six ship tracks and their corresponding source spectra at the closest point of approach (CPA) are shown (section 4.4). The method is confirmed by comparing an

acoustically derived ship track with its AIS track that was available for the car carrier 'Solar Wing'. The directionality of the underwater radiated sound of one ship was characterized with the waist and bow being respectively 3 and 8 dB quieter than the stern of the ship.

4.3 Methods

4.3.1 Experimental Setup

A volumetric hydrophone array coupled to an autonomous acoustic seafloor recorder (Wiggins et al., 2012) was deployed at 1260 m depth in the Southern California Bight (32 22.414' N, 118 33.781' W and recorded data continuously between December 2010 and February 2011 for 63 days at a sampling frequency of 100 kHz (HARP N in chapter 3 and Figure 4.1). The acoustic data was decimated by a factor of 10 for computational efficiency reducing the sampling frequency to 10 kHz.

The volumetric array consists of four hydrophones with spacing ranging from 0.9 m to 1.7 m with the top hydrophone (#1) being 3.5 m above the seafloor (Figure 4.2). The hydrophone sensitivities and transfer function calibrations were performed at the Scripps Whale Acoustics Laboratory and at the U.S. Navy's Transducer Evaluation Center facility in San Diego, California. The minimum of the HARP's peak-to-peak clipping levels between 10 Hz and 10 kHz is 161 $dB\ re\ 1Pa$ at 400 Hz. The location of the HARP and the orientation of its volumetric array were estimated with a root-mean-square (rms) error of 4 m and 3°, respectively, as described in chapter 3 for 'HARP N'.

4.3.2 Ship localization

To estimate directions to surface ships and to investigate potential seafloor reflections, a frequency-domain beamformer (FDB) was implemented (Van Trees, 2002) for the volumetric array configuration defined by its four hydrophone position vectors,

$\mathbf{p}_n = (p_{x_n}, p_{y_n}, p_{z_n})$ with $n = 1..4$ (Figure 4.2). For a given frequency, f, and a vertical and horizontal angle pair, (θ_v, θ_h), the value of the FDB is computed by:

$$B_f = \mathbf{w}_f^H \, \mathbf{R}_f \, \mathbf{w}_f, \tag{4.1}$$

where $\mathbf{w}_f$ is the 4×1 replica vector for the four elements of the array for each angle pair (θ_v, θ_h) and $\mathbf{w}_f^H$ is the Hermitian transpose of $\mathbf{w}_f$. The n-th component of $\mathbf{w}_f$ is obtained by:

$$w_{f_n} = e^{i2\pi f \tau_n(\theta_v, \theta_h)}, \tag{4.2}$$

The time delay, $\tau_n(\theta_v, \theta_h)$, is obtained from the hydrophone position vector $\mathbf{p}_n$ and the direction cosines of a plane wave coming from the direction of (θ_v, θ_h):

$$\tau_n(\theta_v, \theta_h) = -\frac{1}{c} \left[sin(\theta_v)\, cos(\theta_h) \cdot p_{x_n} \, + \, sin(\theta_v)\, sin(\theta_h) \cdot p_{y_n} \, + \, cos(\theta_v) \cdot p_{z_n} \right], \tag{4.3}$$

where c is the local sound speed of 1484 ms^{-1} at the array depth. $\mathbf{w}_f$ was computed for θ_v and θ_h in 1° increments ranging from -90° to +90° and from 0° to 360°, respectively. $\mathbf{R}_f$ in equation 4.1, represents the 4×4 cross-spectral density matrix estimated from 1 s of acoustic data by using a segment length of 256 points and 50% overlap for each of the four channels:

$$\mathbf{R}_f = E\left[\left(\mathbf{X}_f - \boldsymbol{\mu} \right) \left(\mathbf{X}_f^* - \boldsymbol{\mu} \right) \right], \tag{4.4}$$

where $E[\cdot]$ is the expected value and $\mathbf{X}_f$ is a matrix containing the four fast-fourier-transformed (FFT) values of each 256 point long segments for the four hydrophone at the frequency f. $\boldsymbol{\mu}$ is a vector with the mean of the four fast-fourier-transformed (FFT)

values for each segment.

To create an ambiguity surface, FDB values were computed for 145 frequencies with a constant frequency interval between 100 Hz and 1500 Hz and were incoherently averaged for each possible (θ_v, θ_h) pair. The horizontal and vertical angle from the volumetric array to the ship is found at the maximum of the ambiguity surface:

$$max \left\{ \sum_f \left| \mathbf{B}_f \right| \right\} \rightarrow (\theta_{v_s}, \theta_{h_s}) \tag{4.5}$$

Slant ranges, r_s, and horizontal ranges, r_h, from the volumetric array to the ships were obtained from the triangle defined by the location of the ship, volumetric array and the point at the sea surface that is vertically above the array with d representing the hydrophone depth:

$$r_s = \frac{d}{sin(\theta_{v_s})}, \tag{4.6}$$

$$r_h = \frac{d}{tan(\theta_{v_s})}. \tag{4.7}$$

The horizontal ranges, r_h, and their corresponding horizontal angles, θ_{h_s}, are the polar coordinates of the ship locations and were transformed to Cartesian coordinates by:

$$x = r_h \cdot cos(\theta_{h_s}) \tag{4.8}$$

$$y = r_h \cdot sin(\theta_{h_s}), \tag{4.9}$$

where x and y represent the Eastings and Northings geo-referenced to location of the volumetric array.

The magnitude of the speed of the ships, $\|\mathbf{v}_s\|$, was estimated in the vicinity of the CPA as the first derivative of the horizontal ship tracks:

$$\|\mathbf{v}_s\| = \sqrt{\left(\frac{\Delta x}{\Delta t}\right)^2 + \left(\frac{\Delta y}{\Delta t}\right)^2} \tag{4.10}$$

4.3.3 Source spectra and broadband source levels

Power spectral densities (PSDs) in 1 Hz bins were computed from the calibrated acoustic pressure time series recorded on hydrophone #1 by averaging over three consecutive 10,000 point long FFTs with no overlap.

To estimate the source spectra, a spherical propagation model was used, while absorption related losses were considered negligible due to an absorption coefficient of less than 0.1 dB/km for the dominant frequencies of the ship's underwater radiated sound. With the known slant range, r_s in meters, the levels of the source PSD, $SL(f)$, were obtained from the levels of the received PSD, $RL(f)$:

$$SL(f) = 20\,log(r_s) + RL(f) \tag{4.11}$$

Broadband rms source levels in $dB\ re\ 1\mu Pa$ @ 1 m were estimated by integrating the PSD values between 10 Hz and 1 kHz after converting them onto a linear scale:

$$SL\ =\ 10\,log\left(\sum_f 10^{SL(f)\,/\,10}\right). \tag{4.12}$$

4.4 Results

Six ship tracks from SoOs are shown in Figure 4.3 (a) - (f) with track durations and lengths ranging between $11\ -\ 23\ min$ and $5\ -\ 8.5\ km$, respectively. While the ships of track (b), (e) and (f) are heading southwest away from the ports of Los Angeles/Long

Beach by circumnavigating San Clemente Island, the ships of track (c) and (d) are heading eastwards [(c) very closely towards San Diego]. The only ship that neither comes from or heads towards the coast of California is shown in track (a) with a northwest heading. Estimated speeds at CPA for each ship were 8.2, 9.1, 6.3, 9.9, 9.2 and 8.3 ms^{-1} for the tracks (a) - (f), respectively.

The ship of track (d) was identified as the car carrier 'Solar Wing' with gross a tonnage of $41,723\ tons$ (length$\times$width: $190\ m \times 32\ m$) due to the availability of AIS data for this track only. Its GPS-derived AIS track is represented by the thick black line in Figure 4.3 (d) and agrees well with acoustically derived track with deviations between 1.1 and 2.1 of the car carrier's width. A speed of 9.6 ms^{-1} at the CPA was reported by the AIS for 'Solar Wing', which agrees well with the acoustically derived speed of 9.9 ms^{-1}.

The source spectra of each of the six ship tracks estimated at the CPA are shown in Figure 4.4 (a) - (f). In all source spectra, the dominant frequencies are between 10 - 100 Hz as previously found (McKenna et al., 2012). Spectra (a), (b), (e) and (f) decrease dramatically with increasing frequencies between 50 and 100 Hz by several tens of dB, while spectra (c) and (d) decrease less dramatically in this frequency range. Broadband source levels at the CPA ($72° \leq \theta_v \leq 80°$) derived from the spectra for ship tracks (a) - (f) are 198, 193, 190, 192, 191 and 195 $dB\ re\ 1\mu Pa^2\ @1m$, respectively.

A strong dependence of the broadband source level on the vertical angle, θ_v was found for all ship tracks (a) - (f) and will be discussed exemplary for ship track (a) in detail. The broadband source level for ship track (a) as a function of time is shown in Figure 4.5. As the ship approaches the small-aperture array, the broadband source level increases from approximately 190 to about 199 $dB\ re\ 1\mu Pa^2\ @1m$ at the CPA. As the ship passes through the CPA and retreats from the array location, the source level continues to increase up to 202 $dB\ re\ 1\mu Pa^2\ @1m$ in the vicinity of minute 12, and then finally starts to decrease to approximately 199 $dB\ re\ 1\mu Pa^2\ @1m$ at the end of the track.

This is also reflected in the corresponding dependence of the broadband source levels on its vertical angles, θ_v (Figure 4.6). In the approach phase, θ_v increases from 30° to 77°, while the corresponding broadband source level increases from approximately 190 to about 199 $dB\ re\ 1\mu Pa^2\ @1m$. However, as θ_v decreases from 77° to approximately 45° in the retreat phase, the broadband source level continues to increase to about 202 $dB\ re\ 1\mu Pa^2\ @1m$ and decreases only for vertical angles smaller than 45°. Note, that the broadband source level at 45° is about 8 dB higher in the retreat phase than in the approach phase. This strong θ_v - dependence of the broadband source levels and the increased broadband source levels in the retreat phase compared to the approach phase suggest a directionality of the underwater radiated sound of ships with the waist (measured at CPA) and bow (measured during approach) being quieter than the stern (measured during retreat).

For the CPA of ship track (a), the beampattern of the FDB at 386 Hz is shown in Figure 4.7. While the main lobe of the beampattern at $\theta_{v_s} = 77°$ and $\theta_{h_s} = 79°$ reveals the vertical and horizontal angle at the CPA of ship track (a), significant levels of acoustic power reflected off the bottom and received by the small-aperture array would be confined to the lobe peaking at $\theta_v = 258°$ and $\theta_h = -65°$, which is more than 8 dB lower than the main lobe.

4.5 Discussion

Although the accuracy of the ship tracks is sufficient for a horizontal radius of up to 2 km with respect to the small-aperture array, refraction effects decrease the accuracy of the location estimates for horizontal radii greater than 2 km. Hence, instead of triangulating the ranges by assuming straight ray paths, backpropagating the vertical angles from the small-aperture array to the sea surface by using an acoustic propagation model and the measured sound velocity profile (as shown in chapter 3) would improve

the localization accuracy for horizontal ranges greater than 2 km as demonstrated for the shallow-diving killer whales in chapter 2.

The levels of the received spectra of the ships are at least several dB greater than the background noise levels, which decrease from 82 to 58 $dB\ re\ 1\mu Pa^2//Hz$ between 10 Hz and 1 kHz. The variance of the source spectra and broadband source level estimates could be decreased further by averaging over more than 15 segments with 10,000 samples (1 s) each. This could also reduce the variance in the Figures 4.5 and 4.6 that show the broadband source levels as a function of time and θ_v, respectively. (McKenna et al., 2012) used a number of segments determined by the time it would take the ship to travel the distance of its own length. Although the lengths of the ships from all tracks remain unknown due to the absence of AIS data [except for track (d)], the ship lengths might be crudely estimated from the source spectra as some ship types have distinct spectral characteristics [e.g. (McKenna et al., 2012)] allowing the identification of the ship type, which would restrict the range of possible ship lengths.

The broadband source level of 192 $dB\ re\ 1\mu Pa^2$ @ 1 m at the CPA with $\theta_v = 80^\circ$ for the car carrier 'Solar Wing' is 10 - 14 dB higher than previously found for car carriers (McKenna et al., 2012). However, in (McKenna et al., 2012), the broadband source levels were obtained at the CPA with corresponding vertical angles in the vicinity of $\theta_v = 25^\circ$. The broadband source level of 'Solar Wing' for $\theta_v = 25^\circ$ equals 185 $dB\ re\ 1\mu Pa^2$ @ 1 m and is still 3 - 7 dB higher than (McKenna et al., 2012) despite 'Solar Wing' being in its approach phase. However, 'Solar Wing' does travel 1 - 2 ms^{-1} faster than the ships in (McKenna et al., 2012), which could explain the 3 - 7 dB difference (McKenna et al., 2013).

An additional potential contributor to the θ_v - dependence of the broadband source levels could be the ship's radiated acoustic power that reflects off the seafloor and is also received by the small-aperture seafloor array. If acoustic power at negative vertical

angles ($\theta_v < 0°$) in the beampattern at the CPA is present, its levels are lower by more than 2 dB compared to the highest lobe that usually corresponds to the direct path at CPA (Figure 4.7). Since the angular resolution of the FDB is insufficient for the dominant ship frequencies below 100 Hz due to the element spacing of the array, this can only be verified for frequencies greater than 100 Hz and below the minimum spatial Nyquist frequency of 465 Hz.

Due to the array configuration and the measurements of SoOs with no control over their course, the presented method does not fully meet all the criteria for the measurement grade A (precision method) of the standard ASA S12.64-2009/Part 1 for measuring underwater ship sound. However, the simultaneous measurement of the ship source level at three different aspect angles ($\theta_v = 15°, 30°$ and $45°$), which is required for measurement grade A, could be accomplished by deploying two additional single channel recording packages at the seafloor with the hydrophones several or tens of meters above the seafloor. This would allow for measurements of underwater radiated sound from ships 1 km below the noisy surface layer in which multiple natural processes (e.g. surface agitation), contribute to higher ambient noise levels in frequency ranges that overlap with the dominant ship frequency range (Wenz, 1962).

4.6 Conclusions

A method to track ships and to measure their underwater radiated sound with a single autonomous acoustic seafloor package and no AIS data required was described. Six ship tracks and their corresponding source spectra at the CPA ($72° \leq \theta_v \leq 80°$) with broadband source level estimates ranging between 190 and 198 $dB\ re\ 1\mu Pa^2$ @ 1 m are presented. The availability of AIS locations for the ship track (d) verified the method and identified the ship as the car carrier 'Solar Wing' with a broadband source level of 192 $dB\ re\ 1\mu Pa^2$ @ 1 m for $\theta_v = 80°$ at the CPA. The directionality of the underwater radiated

sound was characterized for ship track (a) with the waist and bow being respectively 3 and 8 dB quieter than the stern of the ship.

4.7 Acknowledgments

Chapter 4 is currently being prepared for submission for publication of the material. Gassmann, M., Wiggins, S. M., and Hildebrand, J. A. Tracking and measuring underwater radiated sound from ships with a small-aperture seafloor array. The dissertation author was the primary investigator and author of this paper.

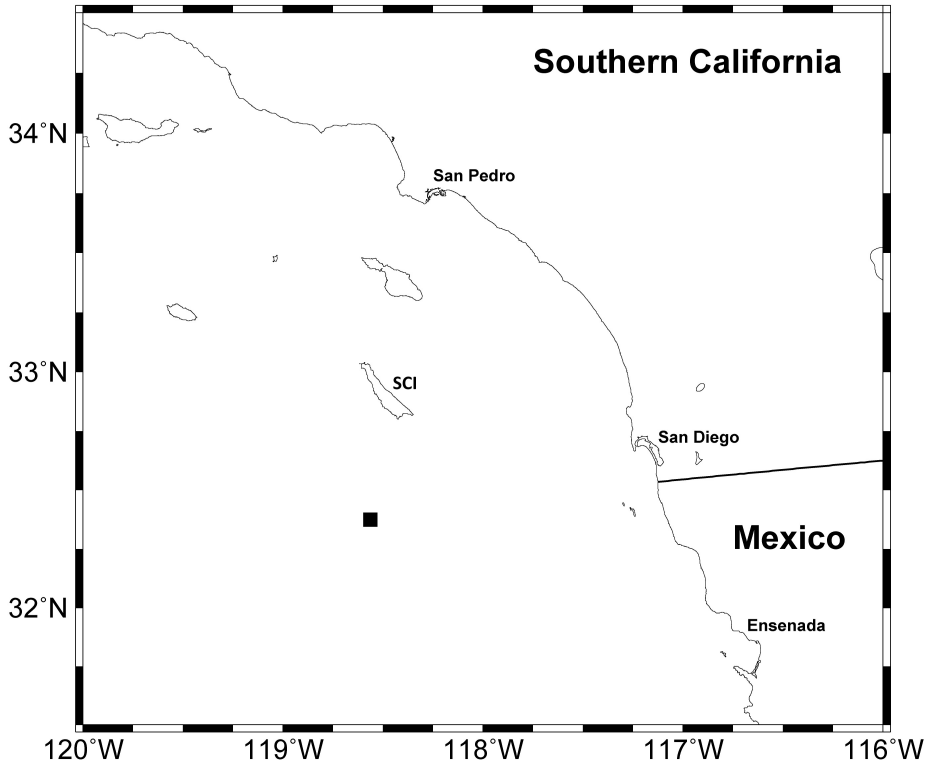

Figure 4.1. Location of the single seafloor instrument with its volumetric small-aperture array (black square at 32 22.414' N, 118 33.781' W) south of San Clemente Island (SCI) in the Southern California Bight at a depth of 1256 *m*. Ports of Ensenada, San Diego and Los Angeles/Long Beach (in San Pedro) are located as shown.

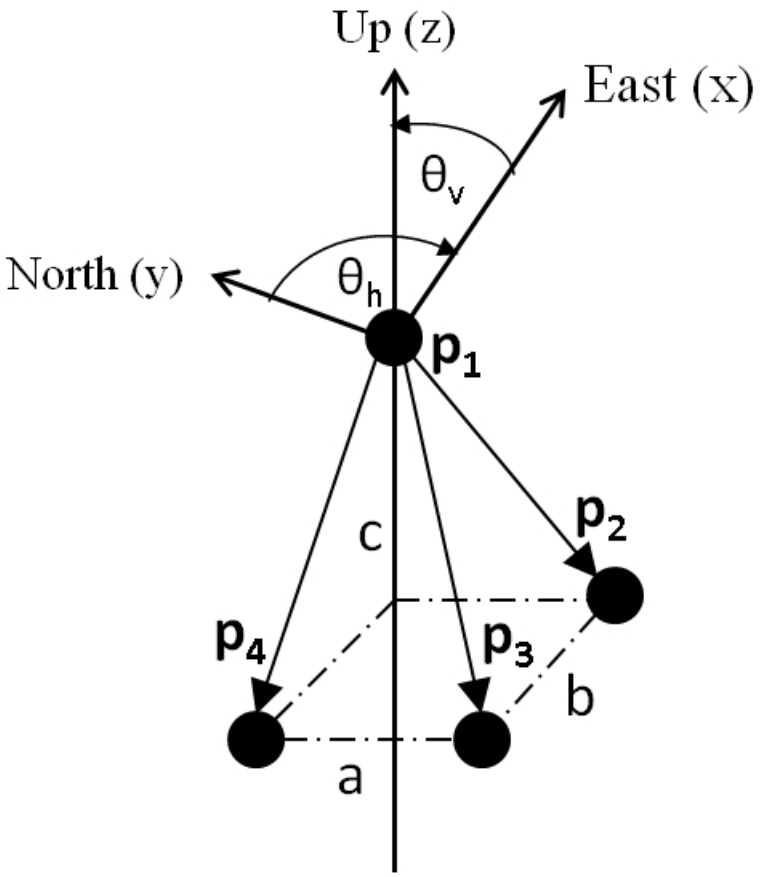

Figure 4.2. Schematic of the volumetric small-aperture array defined by its four hydrophone position vectors $\mathbf{p}_1, .., \mathbf{p}_4$ with spacing $a = 0.9\,m$, $b = 1.1\,m$ and $c = 0.9\,m$. y and x axis are aligned with the northern and eastern cardinal direction. Horizontal angles, θ_h, are measured clockwise with respect to the y-axis with 0° corresponding to North. Vertical Angles, θ_v, are ranging from -90° (straight below $\mathbf{p}_1$) to $+90^\circ$ (straight above $\mathbf{p}_1$).

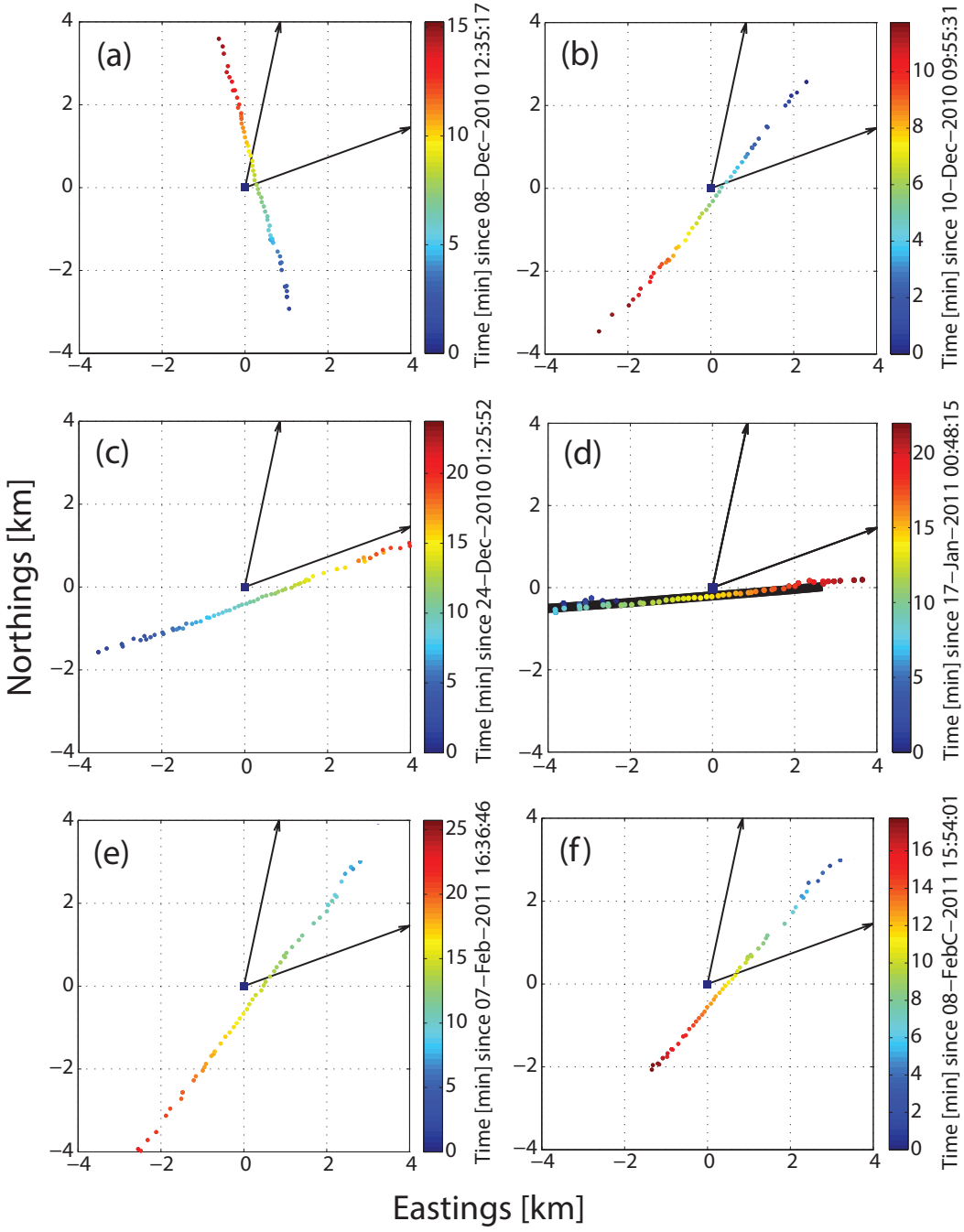

Figure 4.3. Six maps of six individual ship tracks (a) - (f). Estimated ship locations are shown as dots. Color of dots represents time in minutes. The blue square shows the location of the volumetric array. Directions to the port of Los Angeles/Long Beach and San Diego are indicated by the arrows with a magnetic bearing of 12° and 70°, respectively. Thick black line in (d) represents the AIS ship track of the car carrier 'Solar Wing'. Slant ranges to the volumetric seafloor array at the closest point of approach (CPA) for ship tracks (a) - (f) varied between 1.27 *km* and 1.31 *km*.

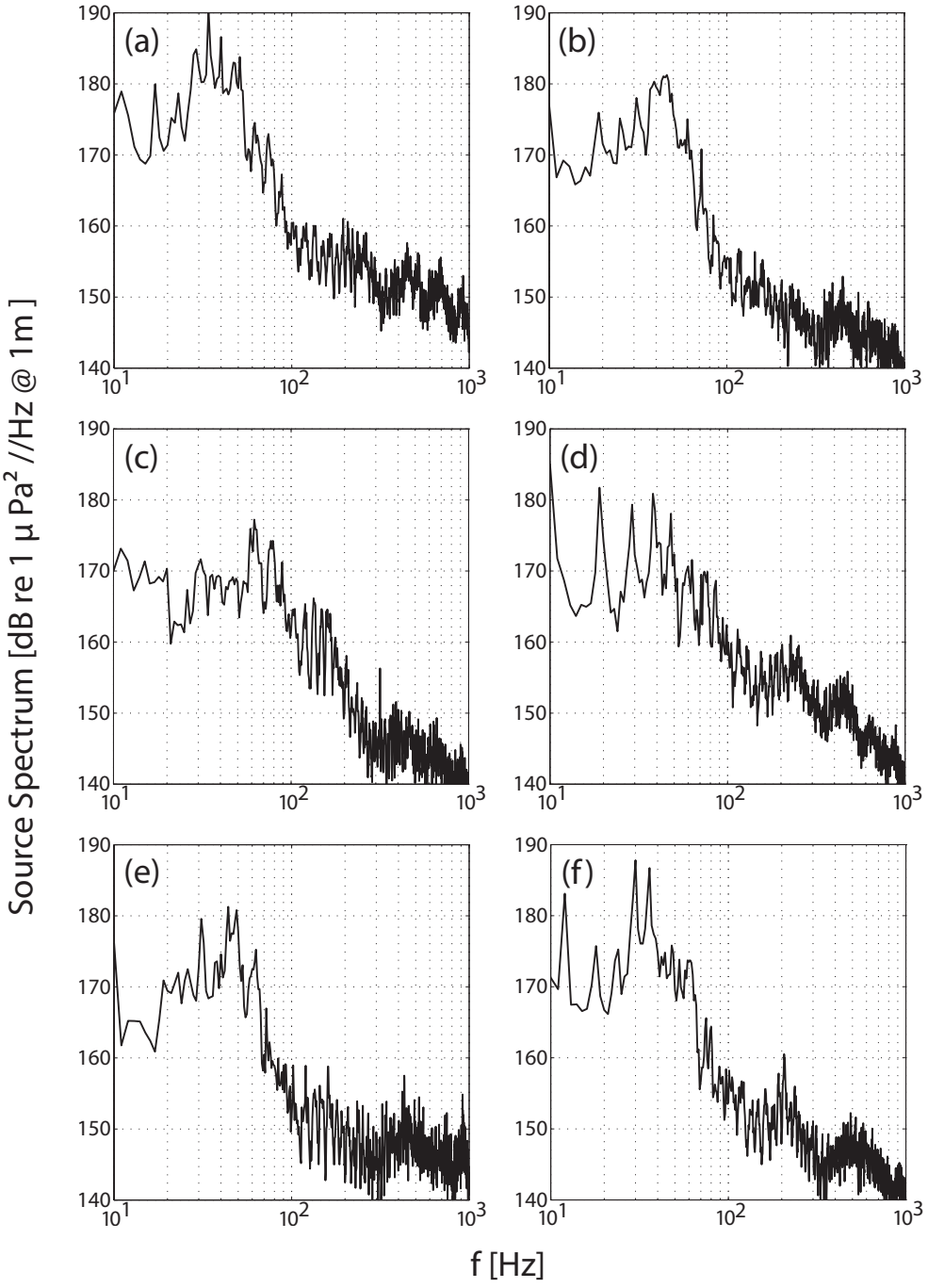

Figure 4.4. Estimated source spectra at the CPA for ship tracks (a) - (f) of Figure 4.3. Corresponding broadband source levels (10 Hz - 1 kHz) for (a) - (f) were 198, 193, 190, 192, 191 and 195 $dB\ re\ 1\mu Pa^2\ @1m$, respectively.

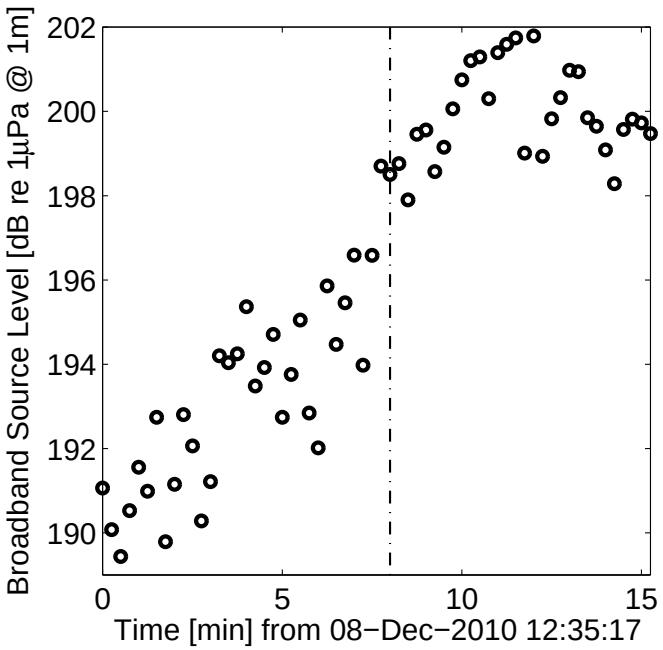

Figure 4.5. Broadband source level as a function of time for ship track (a) of Figure 4.3. Dashed line indicates the time of the CPA with a slant range of 1.29 *km* to the volumetric seafloor array.

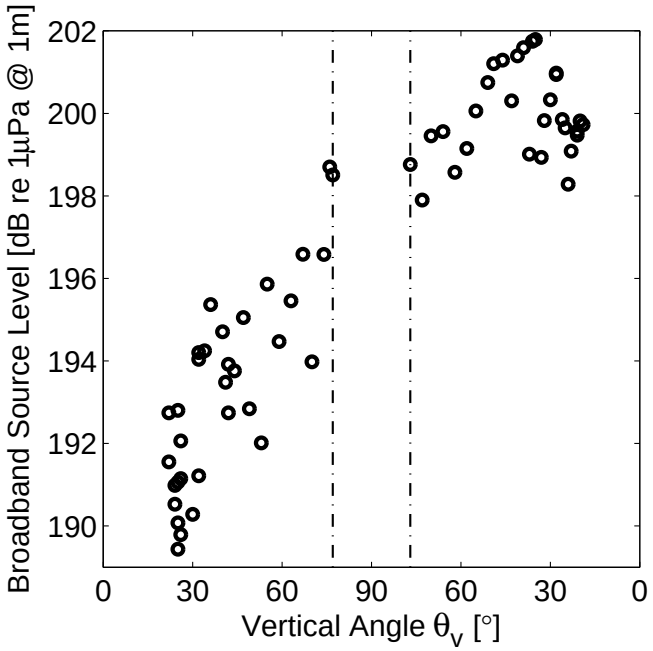

Figure 4.6. Broadband source level as a function of vertical angle, θ_v, for ship track (a) of Figure 4.3. θ_v at CPA is represented by the two dashed lines, which divide the figure into an approach phase (to the left of the left dashed line) and a departure phase (to the right of the right dashed line) with respect to the volumetric seafloor array.

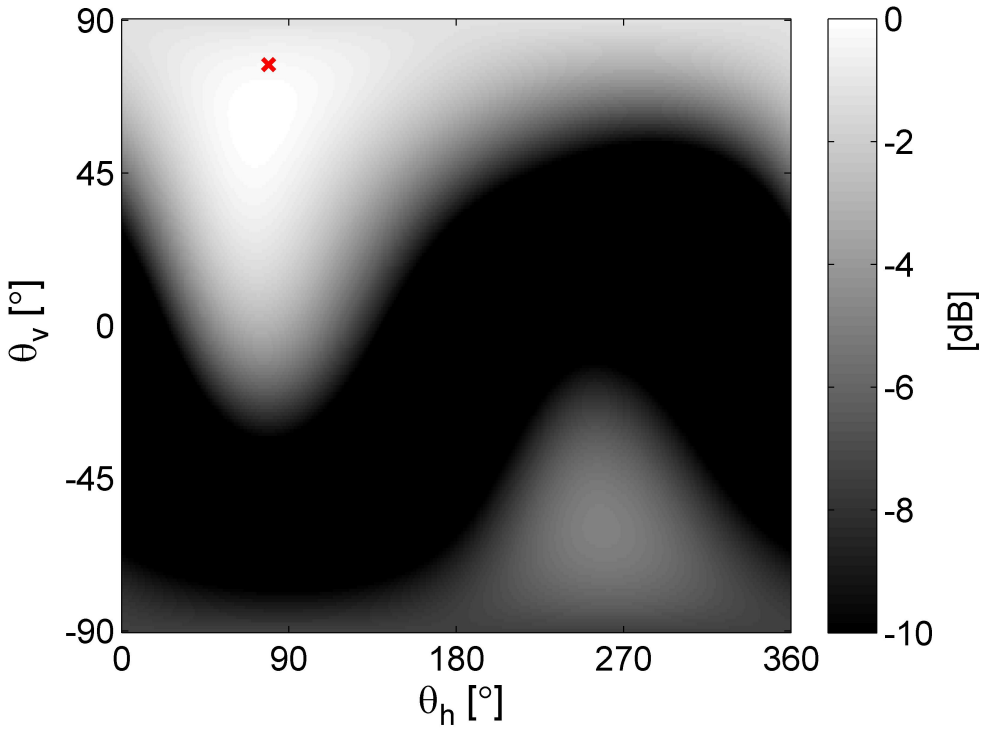

Figure 4.7. Beampattern of the frequency domain beamformer (FDB) at the CPA of ship track (a) from Figure 4.3 for a frequency of 410 Hz. The FDB beampattern was normalized by its maximum for all vertical and horizontal angles, θ_v and θ_h, respectively, and is shown for a dynamic range of 10 dB (greyscale colormap). The beampattern peaks at $\theta_{v_s} = 77^\circ$ and $\theta_{h_s} = 79^\circ$ as indicated by the red cross.

Bibliography

Ainslie, M. and McColm, J. (1998). A simplified formula for viscous and chemical absorption in sea water. *The Journal of the Acoustical Society of America*, 103:1671–1672.

Au, W. W. L. (1993). *The Sonar of Dolphins*. Springer-Verlag, New York.

Au, W. W. L., Ford, J. K. B., Horne, J. K., and Allman, K. A. N. (2004). Echolocation signals of free-ranging killer whales (orcinus orca) and modeling of foraging for chinook salmon (oncorhynchus tshawytscha). *The Journal of the Acoustical Society of America*, 115(2):901–909.

Barlow, J. and Taylor, B. L. (2005). Estimates of sperm whale abundance in the northeastern temperate pacific from a combined acoustic and visual survey. *Marine Mammal Science*, 21(3):429–445. Times Cited: 0 Article English Cited References Count: 28 939xw.

Barrett-Lennard, L. G., Ford, J. K. B., and Heise, K. A. (1996). The mixed blessing of echolocation: Differences in sonar use by fish-eating and mammal-eating killer whales. *Animal Behaviour*, 51(3):553–565.

Baumann-Pickering, S., Roch, M. A., Brownell Jr, R. L., Simonis, A. E., McDonald, M. A., Solsona-Berga, A., Oleson, E. M., Wiggins, S. M., and Hildebrand, J. A. (2014). Spatio-temporal patterns of beaked whale echolocation signals in the north pacific. *PLoS ONE*, 9(1):e86072.

Chen, C.-T. and Millero, F. J. (1977). Speed of sound in seawater at high pressures. *The Journal of the Acoustical Society of America*, 62(5):1129–1135.

Cranford, T. W. (2011). Biosonar sources in odontocetes: considering structure and function. *Journal of Experimental Biology*, 214(8):1403–1404. ISI Document Delivery No.: 739EO Times Cited: 2 Cited Reference Count: 6 Cranford, Ted W. Company of biologists ltd Cambridge.

Cranford, T. W., Mckenna, M. F., Soldevilla, M. S., Wiggins, S. M., Goldbogen, J. A., Shadwick, R. E., Krysl, P., Leger, J. A. S., and Hildebrand, J. A. (2008). Anatomic geometry of sound transmission and reception in cuvier's beaked whale (ziphius cavirostris). *Anatomical Record*, 291(4):353–378.

Del Grosso, V. A. (1974). New equation for the speed of sound in natural waters (with comparisons to other equations). *The Journal of the Acoustical Society of America*, 56(4):1084–1091.

DeRuiter, S. L., Southall, B. L., Calambokidis, J., Zimmer, W. M., Sadykova, D., Falcone, E. A., Friedlaender, A. S., Joseph, J. E., Moretti, D., and Schorr, G. S. (2013). First direct measurements of behavioural responses by cuvier's beaked whales to mid-frequency active sonar. *Biology letters*, 9(4):20130223.

Edds-Walton, P. L. (1997). Acoustic communication signals of mysticete whales. *Bioacoustics*, 8:47–60.

Fisher, F. H. and Spiess, F. N. (1963). Flip-floating instrument platform. *The Journal of the Acoustical Society of America*, 35(10):1633–1644.

Ford, J. K. B. (1989). Acoustic behaviour of resident killer whales (orcinus orca) off vancouver island, british columbia. *Canadian Journal of Zoology*, 67(3):727–745.

Fristrup, K. and Watkins, W. A. (1992). Characterizing acoustic features of marine animal sounds. Report WHOI-92-04, Woods Hole Oceanographic Institution.

Gassmann, M., Elizabeth Henderson, E., Wiggins, S. M., Roch, M. A., and Hildebrand, J. A. (2013). Offshore killer whale tracking using multiple hydrophone arrays. *The Journal of the Acoustical Society of America*, 134(5):3513–3521.

Henderson, E. E., Smith, M. H., Gassmann, M., Wiggins, S. M., Douglas, A. B., and Hildebrand, J. A. (2014). Delphinid behavioral responses to incidental mid-frequency active sonar. *The Journal of the Acoustical Society of America*, 136(4):2003–2014.

Hildebrand, J. A. (2009). Anthropogenic and natural sources of ambient noise in the ocean. *Marine Ecology-Progress Series*, 395:5–20.

Hirotsu, R., Yanagisawa, M., Ura, T., Sakata, M., Sugimatsu, H., Kojima, J., and Bahl, R. (2010). Localization of sperm whales in a group using clicks received at two separated short baseline arrays. *The Journal of the Acoustical Society of America*, 127(1):133–147.

Johnson, M., Madsen, P. T., Zimmer, W. M., De Soto, N. A., and Tyack, P. L. (2004). Beaked whales echolocate on prey. *Proceedings of the Royal Society of London. Series B: Biological Sciences*, 271(Suppl 6):S383–S386.

Kaiser, J. (1990). On a simple algorithm to calculate the "energy" of a signal. In *International Conference on Acoustics, Speech, and Signal Processing*, pages 381–384. IEEE.

Kandia, V. and Stylianou, Y. (2006). Detection of sperm whale clicks based on the teager-kaiser energy operator. *Applied Acoustics*, 67(11-12):1144–1163. Sp. Iss. SI.

Lagarias, J., Reeds, J., Wright, M., and Wright, P. (1998). Convergence properties of the nelder–mead simplex method in low dimensions. *SIAM Journal on Optimization*, 9(1):112–147.

Lewis, T., Gillespie, D., Lacey, C., Matthews, J., Danbolt, M., Leaper, R., McLanaghan, R., and Moscrop, A. (2007). Sperm whale abundance estimates from acoustic surveys of the ionian sea and straits of sicily in 2003. *Journal of the Marine Biological Association of the United Kingdom*, 87(01):353–357.

Madsen, R. T. (2005). Marine mammals and noise: Problems with root mean square sound pressure levels for transients. *The Journal of the Acoustical Society of America*, 117(6):3952–3957.

McKenna, M. F., Ross, D., Wiggins, S. M., and Hildebrand, J. A. (2012). Underwater radiated noise from modern commercial ships. *The Journal of the Acoustical Society of America*, 131(1):92–103.

McKenna, M. F., Wiggins, S. M., and Hildebrand, J. A. (2013). Relationship between container ship underwater noise levels and ship design, operational and oceanographic conditions. *Sci. Rep.*, 3.

Medwin, H. and Clay, C. S. (1998). Fundamentals of acoustical oceanography.

Millero, F. J., Chen, C.-T., Bradshaw, A., and Schleicher, K. (1980). A new high pressure equation of state for seawater. *Deep Sea Research Part A. Oceanographic Research Papers*, 27(34):255–264.

Nosal, E. and Frazer, L. (2007). Sperm whale three-dimensional track, swim orientation, beam pattern, and click levels observed on bottom-mounted hydrophones. *The Journal of the Acoustical Society of America*, 122:1969.

Porter, M. (2005). Bellhop gaussian beam/finite element beam code. *Heat, Light, and Sound Research, Inc., http://oalib.hlsresearch.com/Rays/, Last visited: 1/10/2015*.

Porter, M. B. and Bucker, H. P. (1987). Gaussian beam tracing for computing ocean acoustic fields. *The Journal of the Acoustical Society of America*, 82(4):1349–1359.

Roch, M. A., Klinck, H., Baumann-Pickering, S., Mellinger, D. K., Qui, S., Soldevilla, M. S., and Hildebrand, J. A. (2011). Classification of echolocation clicks from odontocetes in the southern california bight. *The Journal of the Acoustical Society of America*, 129(1):467–75.

Ross, D. (1976). Mechanics of underwater noise.

Samarra, F. I. P., Volker, B. D., Katja, V., Marianne, H. R., Rene, J. S., and Patrick, J. O. M. (2010). Killer whales (orcinus orca) produce ultrasonic whistles. *The Journal of the Acoustical Society of America*, 128(5):EL205–EL210.

Schorr, G. S., Falcone, E. A., Moretti, D. J., and Andrews, R. D. (2014). First long-term behavioral records from cuviers beaked whales (ziphius cavirostris) reveal record-breaking dives. *PLoS ONE*, 9(3):e92633.

Send, U., Visbeck, M., and Krahmann, G. (1995). Aspects of acoustic transponder surveys and acoustic navigation. In *OCEANS '95. MTS/IEEE. Challenges of Our Changing Global Environment. Conference Proceedings.*, volume 3, pages 1631–1642 vol.3.

Shaffer, J. W., Moretti, D., Jarvis, S., Tyack, P., and Johnson, M. (2013). Effective beam pattern of the blainville's beaked whale (mesoplodon densirostris) and implications for passive acoustic monitoring. *The Journal of the Acoustical Society of America*, 133(3):1770–1784.

Simon, M., Wahlberg, M., and Miller, L. A. (2007). Echolocation clicks from killer whales (orcinus orca) feeding on herring (clupea harengus). *The Journal of the Acoustical Society of America*, 121(2):749–752.

Simonis, A. E., Baumann-Pickering, S., Oleson, E., Melcon, M. L., Gassmann, M., Wiggins, S. M., and Hildebrand, J. A. (2012). High-frequency modulated signals of killer whales (orcinus orca) in the north pacific. *The Journal of the Acoustical Society of America*, 131(4):EL295–EL301.

Spiesberger, J. L. and Fristrup, K. M. (1990). Passive localization of calling animals and sensing of their acoustic environment using acoustic tomography. *The American*

Naturalist, 135(1):107–153.

Thode, A. (2005). Three-dimensional passive acoustic tracking of sperm whales (physeter macrocephalus) in ray-refracting environments. *The Journal of the Acoustical Society of America*, 118:3575.

Thode, A., Norris, T., and Barlow, J. (2000). Frequency beamforming of dolphin whistles using a sparse three-element towed array. *The Journal of the Acoustical Society of America*, 107(6):3581–3584.

Thode, A., Skinner, J., Scott, P., Roswell, J., Straley, J., and Folkert, K. (2010). Tracking sperm whales with a towed acoustic vector sensor. *The Journal of the Acoustical Society of America*, 128:2681.

Tiemann, C. O., Thode, A. M., Straley, J., O'Connell, V., and Folkert, K. (2006). Three-dimensional localization of sperm whales using a single hydrophone. *The Journal of the Acoustical Society of America*, 120:2355.

Tyack, P. L., Johnson, M., Soto, N. A., Sturlese, A., and Madsen, P. T. (2006). Extreme diving of beaked whales. *J. Exp. Biol.*, 209:4238–4253.

Van Trees, H. L. (2002). *Detection, Estimation, and Modulation Theory, Part IV, Optimum Array Processing*. Wiley, New York.

Wenz, G. M. (1962). Acoustic ambient noise in the ocean: spectra and sources. *J Acoustic Soc Am*, 34:1936–1956.

Wiggins, S. M., Frasier, K. E., Henderson, E. E., and Hildebrand, J. A. (2013). Tracking dolphin whistles using an autonomous acoustic recorder array. *J. Acoust. Soc. Amer.*, In Press.

Wiggins, S. M. and Hildebrand, J. A. (2007). High-frequency acoustic recording package (harp) for broad-band, long-term marine mammal monitoring. In *International Symposium on Underwater Technology 2007 and International Workshop on Scientific Use of Submarine Cables and Related Technologies 2007*, pages 551–557. Institute of Electrical and Electronics Engineers.

Wiggins, S. M., McDonald, M. A., and Hildebrand, J. A. (2012). Beaked whale and dolphin tracking using a multichannel autonomous acoustic recorder. *The Journal of the Acoustical Society of America*, 131(1):156–163.

Yack, T. M., Barlow, J., Calambokidis, J., Southall, B., and Coates, S. (2013). Passive

acoustic monitoring using a towed hydrophone array results in identification of a previously unknown beaked whale habitat. *The Journal of the Acoustical Society of America*, 134(3):2589–2595.

Zimmer, W. M. X. (2013). Range estimation of cetaceans with compact volumetric arrays. *The Journal of the Acoustical Society of America*, 134(3):2610–2618.

Zimmer, W. M. X., Johnson, M. P., Madsen, P. T., and Tyack, P. L. (2005). Echolocation clicks of free-ranging cuvier's beaked whales (ziphius cavirostris). *The Journal of the Acoustical Society of America*, 117(6):3919–3927. Times Cited: 1 Article English Cited References Count: 32 934oq.